A systematic framework for multidimensional assessment of wake-induced performance heterogeneity in offshore wind farms

Citation for the original published paper (version of record):
Li, M., Song, Y., Cao, G. et al (2026). A systematic framework for multidimensional assessment of wake-induced performance
heterogeneity in offshore wind farms. Applied Energy, 424.
http://dx.doi.org/10.1016/j.apenergy.2026.128501

Applied Energy 424 (2026) 128501

Contents lists available at ScienceDirect

Applied Energy

journal homepage: www.elsevier.com/locate/apen

A systematic framework for multidimensional assessment of wake-induced performance heterogeneity in offshore wind farms

Mingxin Li [a], Yun-Peng Song [b,*], Guiyu Cao [d], Yuka Kikuchi [a], Jonas W. Ringsberg [e], Matthias G.R. Faes [f], Jeom Kee Paik [g], You Dong [h], Jichuan Kang [i], Shen Li [c,*]

[a] Department of Civil Engineering, The University of Tokyo, Tokyo, Japan
[b] Guangdong-Hong Kong-Macao Greater Bay Area Innovation Research Institute, China Communications Construction Company Limited, Zhuhai, Guangdong, China
[c] Department of Naval Architecture, Ocean and Marine Engineering, University of Strathclyde, Glasgow, Scotland, United Kingdom
[d] School of Energy and Power Engineering, Beihang University, Beijing, China
[e] Division of Marine Technology, Department of Mechanical Engineering, Chalmers University of Technology, SE-412 96 Gothenburg, Sweden
[f] Chair for Reliability Engineering, TU Dortmund University, Dortmund, North Rhine-Westphalia, Germany
[g] Department of Mechanical Engineering, University College London, London, England, United Kingdom
[h] Department of Civil and Environmental Engineering, The Hong Kong Polytechnic University, Kowloon, Hong Kong Special Administrative Region of China
[i] College of Shipbuilding Engineering, Harbin Engineering University, Harbin, Heilongjiang, China

HIGHLIGHTS

- The wake effect is reframed as a lifecycle heterogeneity problem in offshore wind farms.
- A framework is developed to integrate wake aerodynamics, structural integrity, and maintenance management.
- The cross-scale propagation of wake-induced local differences into farm-level performance divergence is revealed.
- The study provides a new perspective for wake effect evaluation in terms of performance and asset management.

GRAPHICAL ABSTRACT

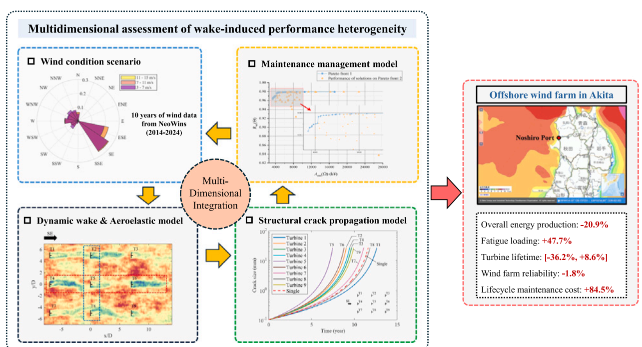

ARTICLE INFO

Keywords:
Offshore wind farms
Wake effects
Lifecycle management
Energy production
Structural integrity
Operations and maintenance

ABSTRACT

Assessment of the wake effect in offshore wind farms has long focused on power production and fatigue loading. However, wake interactions can propagate and accumulate throughout long-term operations, leading to broader inter-turbine heterogeneity, including structural degradation, maintenance requirements, and lifecycle costs. This cross-layer effect and its wider implications remain unexplored in existing studies. To address this gap, this study develops a systematic framework for the multidimensional assessment of wake-induced performance heterogeneity at the wind farm level. The conceptual contribution of the framework is to link wake aerodynamics, structural integrity analysis, and maintenance management within a unified analytical chain. Specifically, turbine-specific operating conditions and loading histories under wake effects are first characterized, then translated into crack-growth trajectories and reliability evolution, and finally incorporated into lifecycle O&M optimization. A representative case study of an offshore wind farm in Akita, Japan, is conducted to demonstrate the applicability of the framework. For the investigated case, the results show that wake-induced heterogeneity reduces overall

* Corresponding authors.
Email addresses: songyunpeng@cccltd.cn (Y.-P. Song), shen.li@strath.ac.uk (S. Li).

https://doi.org/10.1016/j.apenergy.2026.128501
Received 8 April 2026; Received in revised form 16 June 2026; Accepted 16 July 2026
Available online 22 July 2026

energy production efficiency by 20.9%, increases fatigue loading by 47.7%, induces structural lifetime variations from −36.2% to + 8.6% across turbines, lowers wind turbine reliability by 1.8%, and increases lifecycle maintenance costs by 84.5%. By advancing wake analysis from local aerodynamic assessment to a broader perspective on wind farm performance and asset management, the study supports more informed project evaluation and long-term planning for offshore wind farms.

1. Introduction

1.1. Background

Driven by the global pursuit of carbon neutrality, the transition to renewable energy sources is accelerating to realize net zero carbon emissions [1–3]. As a rapidly maturing renewable energy technology, offshore wind energy is becoming a cornerstone of future clean energy [4,5]. As of 2022, the cumulative global offshore wind capacity had reached nearly 70 GW [6], and this figure is expected to rise to over 400 GW by 2032 [7]. Against this rapid expansion, wake interactions within offshore wind farms have emerged as a critical challenge to the efficient and sustainable utilization of wind energy. Shaped by turbine layout, wake effects create non-uniform inflow conditions across the farm, typically characterized by reduced wind speed and elevated turbulence intensity in downstream regions [8,9]. As a result, turbines are exposed to markedly different aerodynamic environments, thereby giving rise to wake-induced performance heterogeneity.

In this study, the wake-induced performance heterogeneity refers to the turbine-to-turbine multidimensional disparities induced by wake effects over the long-term operation of turbines, as manifested in load histories, energy production efficiency, structural degradation, maintenance requirements, and long-term asset performance. On the one hand, when an upstream turbine extracts kinetic energy from the incoming flow, it leaves behind a slower and more turbulent wake, causing downstream turbines to produce persistently less power and thereby reducing the farm-level energy yield. This aspect has been widely examined and remains the dominant focus of existing wake-effect studies [10–13]. On the other hand, the same non-uniform inflow conditions induce substantial inter-turbine variability in structural loading, which can lead to turbine-specific differences in fatigue crack growth, degradation evolution, and the reliability of support structures [14–16]. These longer-term consequences are particularly important for offshore wind turbines, where failure rates are relatively high and failure consequences are often severe due to the harsh marine environment and costly repair logistics [17–19]. However, compared with the extensive literature on wake-induced power losses and fatigue loading, the broader manifestations of wake-induced heterogeneity remain much less understood.

Evidence from practice further highlights the significance of this issue. At the Lillgrund offshore wind farm in Sweden, more than a decade of SCADA data revealed power losses of up to 28% due to turbine clustering and wake interactions [20]. In Japan, the investigation report on the 2023 Rokkasho Tower collapse also indicated that fatigue induced by aerodynamic loading, together with inadequate maintenance, may have been among the contributing causes of the accident [21]. These practical cases suggest that wake effects may have implications beyond local aerodynamic losses and therefore deserve a broader wind farm-level assessment.

1.2. Literature review

Because wake-induced performance heterogeneity in offshore wind farms involves multiple interconnected aspects, the existing literature needs to be critically reviewed from three key perspectives, namely wake aerodynamics, structural integrity, and maintenance management. Such a connected review is necessary to identify the knowledge gaps that remain in existing studies in addressing this issue, thereby motivating the proposed methodology in this study.

1.2.1. Wake aerodynamics in offshore wind farms

Wind turbine wakes affect wind farm performance by reducing inflow velocity and increasing turbulence for downstream turbines, thereby causing power deficits that depend on wake alignment, turbine spacing, and atmospheric conditions. Over the past two decades, extensive research has been devoted to aerodynamic wake effects and their implications for power production and turbine loading. A wide range of wake modeling approaches has been developed, including analytical engineering models such as Jensen and Larsen, the Dynamic Wake Meandering (DWM) framework [22–24], high-fidelity large-eddy simulation (LES) tools such as SOWFA [25–28], and mid-fidelity tools such as FAST.Farm. These studies have substantially advanced the understanding of wake flow dynamics and their effects on farm-level energy yield and structural loading [29–31].

However, the existing literature remains limited in two important respects. First, the fatigue analysis often relies on simplified wake representations that neglect the spatiotemporal variability of wake-induced inflow fields. High-fidelity CFD methods, including LES and Unsteady Reynolds-Averaged Navier–Stokes (URANS), can resolve wake structure, turbulence transport, and wake–wake interactions with high accuracy, but their computational cost is prohibitive for long-term fatigue assessment and large-scale wind-farm analysis [27,32]. By contrast, traditional static engineering wake models are computationally efficient, but they cannot capture dynamic wake evolution or the resulting unsteady load fluctuations on downstream turbines. DWM-based models therefore provide an important compromise [33,34], yet early implementations still relied on empirical parameterizations and quasi-steady assumptions for wake shape and deficit evolution [22–24,35]. Similarly, IEC 61400–1 [36] typically represents wakes as uniformly distributed velocity deficits, neglecting important features such as non-uniform shear, lateral asymmetry, and dynamic meandering [37–39]. Recent developments have improved the physical description of wake kinematics by explicitly accounting for wake propagation velocity and deflection [31,35]. In parallel, high-fidelity simulations have shown that fatigue loads vary markedly with turbine position within the wake, producing pronounced spatial heterogeneity in structural response [29,40,41]. Comparative studies further indicate that uniform wake models may systematically underestimate fatigue loads relative to spatially resolved approaches [29,30]. In large offshore wind farms, this issue becomes even more critical because multi-wake overlap, merging, and interference generate highly dynamic flow structures that static or quasi-steady models cannot adequately represent. Recent efforts on wake-merging formulations under heterogeneous inflow conditions [26,42,43] point toward more realistic yet computationally tractable solutions. Second, existing studies remain largely focused on aerodynamic effects and load analysis. The subsequent link from wake-induced inflow and loading differences to turbine-specific fatigue damage, structural deterioration, and reliability evolution has not yet been systematically established.

1.2.2. Structural integrity of offshore wind structures

In the structural integrity assessment of offshore wind structures subjected to fatigue damage, most existing studies have focused on assessments based on S–N curves [44–46]. Representative examples include the S–N-based fatigue assessment of a 5 MW offshore wind turbine with a gravity-based foundation by Velarde et al. [47], the long-term fatigue analysis of multi-planar tubular joints in jacket-type offshore wind turbines by Dong et al. [48], and the long-term fatigue damage assessment of a floating offshore wind turbine by Li and Zhang [49], where a C-vine copula model was used for multivariate environmental characterization. Further applications of S–N-curve-based fatigue assessments in offshore wind structures have also been reported in [50–54]. These studies have provided an important basis for fatigue evaluation under offshore environmental loading.

However, although the S–N approach is widely accepted in engineering practice [55], it remains limited in its ability to support integrity management and maintenance planning, especially when simulated damage needs to be compared with inspection findings for model updating [56]. This limitation arises because S–N-based methods typically provide only a notional damage index rather than a directly interpretable physical damage state. For this reason, fracture-mechanics-based approaches are more suitable for representing fatigue crack propagation and damage evolution in a physically meaningful manner [57–61]. In parallel, Engineering Critical Assessment (ECA) methods have been increasingly used to evaluate the damage tolerance of cracked structures [62,63]. Compared with S–N-based formulations, these approaches provide a stronger basis for linking structural condition assessment with integrity-informed maintenance.

Nevertheless, wake effects remain weakly integrated into the structural integrity literature. As discussed in Section 1.2.1, wake interactions within offshore wind farms create spatially varying inflow conditions and hence differentiated fatigue loading across turbines. Such differences are expected to lead to non-uniform deterioration and reliability evolution among turbine support structures. Yet most existing structural integrity studies still assess fatigue damage at the individual-turbine level or under simplified loading assumptions, without explicitly incorporating wake-induced inter-turbine heterogeneity into crack growth and integrity evaluation. Although Zhang et al. [64] recently examined the influence of turbine interactions and wake steering control on fatigue loading at the blade root, the linkage between wake-induced loading heterogeneity, fracture-mechanics-based fatigue evaluation, and the resulting implications for structural deterioration and maintenance planning remains largely unexplored.

1.2.3. Maintenance management for offshore wind turbines

From the perspective of maintenance management, offshore wind turbine O&M has gradually evolved from traditional time-based maintenance toward condition-based and health-informed strategies, driven by advances in sensing and Industry 4.0 technologies [65–71]. Various sensing techniques have been used to collect structural condition data [72–74], which are then analyzed to characterize damage-related states [75–77]. On this basis, current health conditions can be assessed and future states predicted, thereby supporting maintenance decision-making [78,79]. Such a lifecycle-oriented integration of monitoring, diagnosis, prognosis, and maintenance decision-making is recognized as the concept of Digital Healthcare Engineering (DHE) [76,80]. Recent research in this area has mainly focused on structural health monitoring (SHM) [81–84], damage detection and prognostics enabled by big data and AI techniques [85–87], and maintenance decision-making informed by structural health assessment [88,89]. These developments have substantially improved the ability to translate structural condition information into maintenance actions.

However, the existing maintenance literature remains limited in three important respects. First, wake-induced load variations can lead to differentiated degradation states, such as cracks, across turbines, yet most existing studies still focus on individual wind turbine structures without accounting for inter-turbine heterogeneity in degradation and the corresponding maintenance implications [88,90,91]. As a result, maintenance strategies formulated from a single-turbine perspective may neglect the collective health states of turbines across the wind farm, which is increasingly inadequate for large-scale offshore wind developments. Second, economic dependence among turbines creates opportunities for grouped or opportunistic maintenance and thus for reducing O&M costs [92–97]. Although such strategies have been applied to nacelle components [98], their application to fatigue-sensitive structural elements under heterogeneous degradation conditions remains largely unexplored. This limits the ability of current studies to capture how wake-induced differences in structural condition may reshape wind-farm-level maintenance coordination. Third, maintenance optimization for offshore wind turbine structures is still commonly formulated with a single objective, such as cost [88], reliability [99,100], or risk [101,102]. However, maintenance planning under wake-induced heterogeneity requires a more integrated perspective that can simultaneously account for multiple lifecycle objectives and the coupled consequences of differentiated structural conditions across turbines [103].

Overall, although existing studies have advanced monitoring, prognostics, and maintenance optimization for offshore wind turbines, they still lack a wind-farm-level perspective that explicitly incorporates wake-induced heterogeneity in structural condition and its implications for coordinated, lifecycle-oriented maintenance decision-making.

1.3. Novelty of this paper

The above review reveals a critical knowledge gap. Existing studies have provided important insights into wake aerodynamics, structural integrity, and maintenance management, but these aspects have mostly been examined separately. As a result, it remains insufficiently understood how wake-induced differences in local inflow conditions and loading histories propagate across turbines and accumulate into wind farm-level consequences, including energy production loss, fatigue loading variation, structural deterioration, reliability changes, and lifecycle O&M performance. This lack of understanding not only obscures, from a scientific perspective, the cross-layer mechanism through which local and short-term wake-induced differences evolve into system-level and lifecycle consequences, but also limits, in practice, more realistic long-term performance assessment and lifecycle management of offshore wind farms.

To address the above gap, this study develops a systematic framework for the multidimensional assessment of wake-induced heterogeneity in offshore wind farms. Rather than examining wake aerodynamics, structural degradation, and maintenance decision-making in isolation, the proposed nexus-driven framework links these processes within a unified analytical chain to reveal how wake effects propagate through wind-farm operation and translate into broader lifecycle consequences. Specifically, the framework first characterizes turbine-specific inflow conditions and loading histories under wake interactions based on long-term site wind statistics. It then maps these loading differences into turbine-level degradation evolution and structural reliability changes. Finally, the resulting heterogeneity in structural health is incorporated into maintenance planning to evaluate its implications for lifecycle reliability and O&M cost performance. An integrated perspective is provided for understanding how wake-induced heterogeneity affects both energy production and long-term asset management at the wind-farm level.

In summary, the novelty and contributions of this study are:

(1) To move beyond conventional wake effect studies centred on power loss and fatigue loading, this study reconceptualizes wake effects in offshore wind farms as a multidimensional heterogeneity problem with broader implications for wind farm reliability, maintenance management, and long-term asset performance.
(2) A systematic framework is established by coupling wake aerodynamics, structural integrity analysis, and maintenance management, enabling wake-induced differences to be traced consistently from local operating conditions to farm-level lifecycle consequences.
(3) The resulting analysis supports more realistic evaluation of offshore wind farm performance from both energy production and

lifecycle management perspectives, thereby informing long-term asset management and planning.

1.4. Outline

The remainder of this paper is organized as follows. Section 2 presents the proposed methodology and introduces the constituent models within the overall framework. Section 3 presents a representative case study based on an offshore wind farm located in Akita, Japan. The results verify the feasibility of the proposed methodology and emphasize its advantages through comparative analysis. Concluding remarks are provided in Section 4.

2. Methodology

In this section, we first present the overall framework of the proposed approach, which integrates three key models including a dynamic wake effect model, a structural crack propagation model, and an O&M optimization model. Subsequently, each individual model is introduced to highlight the specific methods employed to address the corresponding problems. The integration of these models is demonstrated through a nexus-driven coupling structure, enabling the consistent flow of information from aerodynamic loading to structural degradation and maintenance decision-making.

2.1. Overall framework

To systematically address the interdependent challenges of wake-induced loads, fatigue-driven structural degradation, and cost-reliability trade-offs in offshore wind farm O&M, this study develops a nexus-driven framework that integrates three individual models, as illustrated in Fig. 1.

The three interconnected models are briefly introduced below.

(1) **Wake effect model:**
This model begins by evaluating site-specific wind conditions through the construction of joint probability distributions (JPDs) of wind speed and wind direction, derived from long-term historical measurements. These distributions serve as input to a dynamic wake and aeroelastic simulation model, which integrates turbulent flow fields, wind turbine layout, and structural response characteristics. By iteratively updating the inflow conditions of each turbine using a dynamic wake meandering model, this model generates turbine-specific time-series of inflow velocities and associated structural loading histories, thereby capturing spatially and temporally varying wake effects under realistic operating scenarios.

(2) **Crack propagation model:**
As the wake-structure nexus, the wind speed and direction, together with turbine-specific loading histories are then fed into a physics-based crack growth model, which evaluates fatigue-induced damage accumulation using Paris' law and fracture mechanics principles. The model simulates the crack propagation under variable-amplitude cyclic loading, and identifies the point at which a critical crack size is reached, marking potential failure. To account for uncertainty in material properties, loading conditions, and model parameters, a probabilistic ECA model is embedded, which samples relevant stochastic variables and computes the probability of failure or reliability index as a function of crack size. This model establishes a mechanistic link between dynamic loading and degradation trends, enabling predictive assessment of structural health evolution over time.

(3) **O&M decision-making model:**
The Paris' law-based crack growth and reliability degradation trend are input into the O&M optimization model as the structure-maintenance nexus. These structural degradation indicators are utilized within a condition-based opportunistic maintenance model that continuously compares the predicted crack sizes with predefined maintenance thresholds. Once the degradation exceeds the trigger threshold, the model triggers feasible maintenance types and schedules. A multi-objective optimization model is formulated to determine the optimal inspection and maintenance strategy by balancing competing goals, namely minimizing O&M costs and maximizing structural reliability, while adhering to physical and operational constraints such as maximum allowable crack sizes.

Overall, in this framework, the information flow proceeds sequentially across the three models. The wake effect model first provides turbine-specific inflow and structural loading histories under each wind speed and wind direction condition. These loading histories are then converted into stress histories and equivalent stress ranges in the crack propagation model, from which crack-growth trajectories and reliability

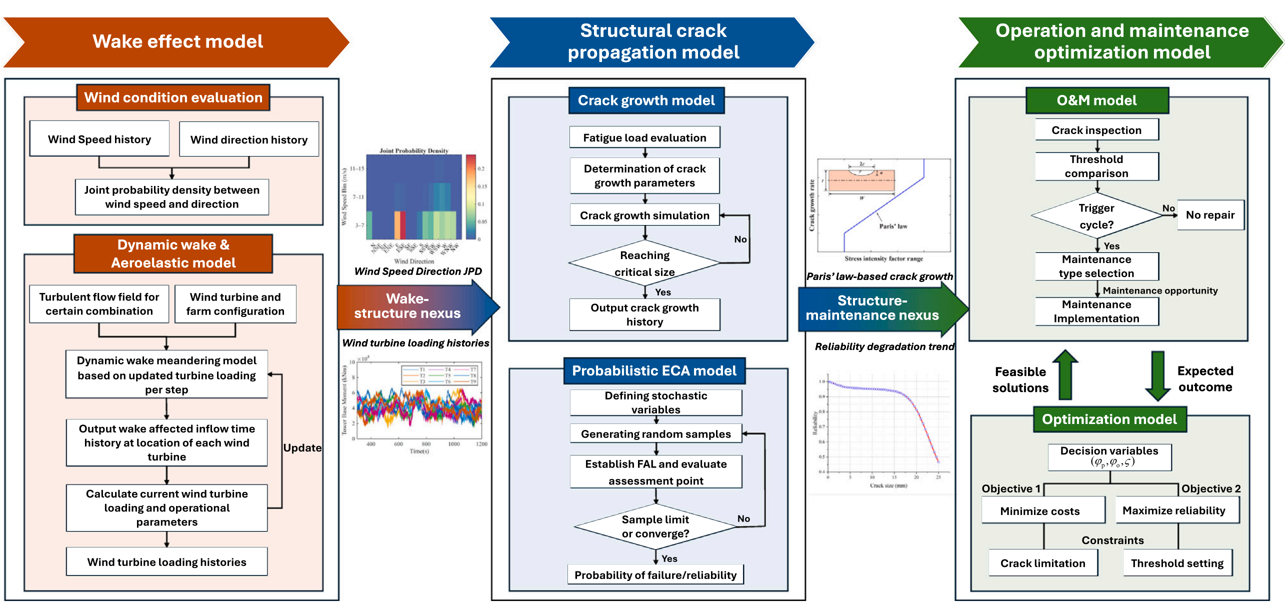

Fig. 1. Overall nexus-driven framework for offshore wind turbines.

indices are obtained for each turbine. Finally, the turbine-specific degradation and reliability states are transferred to the O&M model as state variables for threshold comparison, maintenance triggering, and multi-objective optimization.

2.2. Dynamic wake-aeroelastic model

This section outlines the methods used to simulate wind turbine loading under wake-affected inflow conditions. Three complementary components are employed: an inflow statistical model, which characterizes representative wind states through joint probability distributions; an aeroelastic model, which resolves turbine structural responses under stochastic inflows; and a dynamic wake model, which accounts for wake meandering, expansion, and added turbulence.

2.2.1. Inflow statistics and modeling

In this study, the characterization of inflow conditions is based on a JPD of wind speed and wind direction, constructed from long-term offshore wind resource data. The wind direction is discretized into 16 equally spaced sectors over 360 degrees. For each direction, the wind speed is categorized into three operational regimes: below-rated (3–7 m/s), around-rated (7–11 m/s), and above-rated (greater than 11 m/s). This categorization is designed to reflect the nonlinear behavior of wind turbine loading across different control regions, while maintaining computational tractability. In total, this yields 48 wind-state combinations.

The use of only three wind speed bins strikes a balance between modeling fidelity and computational efficiency. Each regime corresponds to a fundamentally different turbine response: the below-rated regime involves increasing thrust under fixed-pitch control, the around-rated regime exhibits significant variability due to rapid control transitions, and the above-rated regime features pitch-dominated regulation with reduced mean thrust but persistent turbulence-induced fluctuations. Grouping the inflow conditions in this way enables the model to preserve key mechanical characteristics across operating states without being burdened by excessive combinatorics.

For each of the 48 combinations, a full-field three-dimensional turbulent inflow was generated using TurbSim, configured with IEC Class C turbulence intensity and neutral atmospheric stability. Each inflow realization had a total duration of 720 s. The first 120 s was reserved as an initial transient period in the subsequent OpenFAST simulation and was excluded from post-processing. Therefore, only the final 600 s, corresponding to a 10 min turbulent inflow sample, was used for calculating turbulence statistics, mean values, and fatigue loads. The mean wind speed prescribed in each TurbSim simulation was set to the average value within the corresponding wind-speed bin, ensuring consistency with the joint probability distribution.

The resulting turbulent inflows are used as input for FAST.Farm, which simulates the dynamic aeroelastic response of each wind turbine under the given wind state. Time histories of the tower base fore-aft bending moment at all load cases are extracted from the simulations and passed to the structural integrity assessment model for stress analysis and crack propagation simulation. The contribution of each load case to fatigue crack growth is probabilistically aggregated as detailed in Section 2.3.

This modeling approach enables a statistically and physically representative characterization of wind turbine inflow conditions, tailored for integration with dynamic wake effects and structural fatigue models. The methodology is consistent with IEC 61400–1 design standards [36], and is supported by recent findings emphasizing the importance of joint probability-based inflow representation for accurate fatigue load estimation in offshore wind environments [29,30].

In the present study, the annual distribution of daily averaged wind speed was used to characterize the long-term wind climate and to identify representative mean wind speed bins for fatigue analysis. It should be noted that the daily averaged wind speed was not directly used as the inflow time series for turbine load calculations. Instead, for each selected representative mean wind speed condition, a 10 min turbulent inflow field was generated according to the IEC turbulence model, and the turbine loads and corresponding damage equivalent loads (DELs) were evaluated from these turbulent simulations. Therefore, the effects of short-term turbulence fluctuations, small-scale gusts, and the associated load peaks were inherently included in the fatigue assessment for each representative operating condition.

2.2.2. Aeroelastic model

To assess the coupled aeroelastic response of each wind turbine under dynamically evolving wake conditions, this study utilizes OpenFAST, an open-source, high-fidelity, nonlinear aero-servo-hydro-elastic simulation tool developed by NREL. OpenFAST models the structural and control response of wind turbines by solving the equations of motion for flexible components such as blades and towers, under the influence of unsteady aerodynamic loads and operational control actions.

OpenFAST is embedded within the mid-fidelity FAST.Farm framework to simulate wake interactions across the full wind farm. FAST.Farm integrates turbine-level OpenFAST solvers with a computationally efficient implementation of the dynamic wake meandering model. This enables the simulation of wake advection, diffusion, and merging on a coarser farm-scale grid, while each turbine's rotor is resolved on a fine time scale using blade element momentum (BEM) theory and dynamic inflow models. Compared to high-resolution CFD such as LES, this approach achieves significant computational efficiency (up to 100× faster) while maintaining physically consistent aeroelastic fidelity.

For each wind direction sector and wind speed bin, IEC Class C neutral inflow conditions are generated using TurbSim, which produces spatially coherent, 3D stochastic wind fields. These full-field inflows are input into FAST.Farm, ensuring complete consistency between the turbulence characteristics, wake development, and resulting turbine responses. To maintain methodological consistency, the generalized added turbulence model is employed with fixed parameters across cases, controlling wake growth rate, meander filtering length scale, and turbulence intensity.

In this study, two key outputs from OpenFAST are extracted for each turbine under each inflow condition.

(1) Tower base fore-aft bending moment: Used as the primary input for downstream fatigue analysis and crack propagation modeling, forming the structural loading basis in the fracture mechanics model. This location is selected because the tower base typically experiences the maximum bending stresses induced by aerodynamic thrust and gravitational loads, making it the most critical section for fatigue assessment and structural integrity evaluation according to IEC 61400–1 and established industry practice. Other critical locations, including the transition piece and the monopile, are beyond the present scope of this study and will be examined in future work as the model is extended.
(2) Electrical power output: Used to evaluate the energy production and assess potential revenue loss due to wake-induced performance degradation.

By incorporating these outputs into a probabilistic framework, the model captures the spatial and temporal heterogeneity of turbine loading and power generation induced by complex wake dynamics. This aeroelastic simulation thus serves as the critical interface linking aerodynamic wake effects to structural degradation and O&M optimization. For the subsequent structural integrity analysis, the tower base fore-aft bending moment histories are transferred as the load input for stress range calculation and crack propagation simulation, while the corresponding wind state probabilities are used to aggregate fatigue contributions across the considered inflow conditions.

2.2.3. Dynamic wake model

By embedding the dynamic wake meandering formulation within the aeroelastic loop and driving it with realistic turbulence inflow, this model enables (i) evaluation of controller-induced transient responses under evolving wakes, (ii) quantification of the incremental fatigue damage caused by wake-added turbulence (WAT) in multi-wake interactions, and (iii) scalable probabilistic lifetime assessment across the wind farm. This integrated framework thus bridges the gap between computational efficiency and physical accuracy in fatigue load estimation for offshore wind farms.

In this study, FAST.Farm is used to evaluate the fatigue loading of each wind turbine under complex wake interactions. Each turbine m is located at coordinates (x_m, y_m, z_m) in the wind farm layout as demonstrated in Fig. 9, and its wake is modeled individually while dynamically interacting with the wakes of upstream turbines.

In FAST.Farm, each wind turbine is simulated at fine temporal resolution, while the downstream wake is discretized into evolving planar sections (wake planes) that are convected, diffused, and merged over a coarser grid. This results in a computational cost approximately two orders of magnitude lower than full LES while preserving the fidelity of the BEM theory.

For turbine m, the time-varying wake centerline positions in the lateral and vertical directions are modeled as

$$\begin{aligned} y^m_{\mathrm{md}}(t) &= \int_0^t \mathcal{A}^m(\tau)\, b'_{y,m}(\tau)\, d\tau, \\ z^m_{\mathrm{md}}(t) &= \int_0^t \mathcal{A}^m(\tau)\, b'_{z,m}(\tau)\, d\tau, \end{aligned} \tag{1}$$

where $b'_{y,m}$ and $b'_{z,m}$ are the transverse and vertical turbulent fluctuations at the rotor center of turbine m, and $\mathcal{A}^m(\tau)$ is a temporal filter representing the wake meandering coherence of that turbine.

The instantaneous velocity deficit within the wake of turbine m is assumed to follow a super-Gaussian distribution:

$$\Delta\Xi^m(x,y,z,t) = \Delta\Xi^m_{\max}(x')\, \exp\left\{ -\left[\frac{(y - y^m_{\mathrm{md}}(t))^2 + (z - z^m_{\mathrm{md}}(t))^2}{2\,\varrho^m(x')^2} \right]^{n^m} \right\}, \tag{2}$$

where $x' = x - x_m$ is the downstream distance relative to turbine m, $\Delta\Xi^m_{\max}(x')$ is the peak velocity deficit, $\varrho^m(x')$ is the wake width, and n^m is a shape parameter (typically $1.5 \le n^m \le 2$).

The wake expansion is modeled as

$$\varrho^m(x') = \varrho^m_0 + k^m_{\mathrm{wg}} x', \tag{3}$$

where ϱ^m_0 is the initial wake width and k^m_{wg} is the wake growth rate.

To account for WAT, the model introduces an additional turbulence intensity following the generalized added turbulence formulation:

$$\iota^m_{\mathrm{added}}(x') = \iota^m_{\mathrm{az}} \left(1 - \exp\left[-\frac{x'}{\mathcal{E}^m_{\mathrm{az}}} \right] \right), \tag{4}$$

where ι^m_{az} is the asymptotic added turbulence and $\mathcal{E}^m_{\mathrm{az}}$ is the meander filtering length scale. For methodological consistency, these parameters are typically kept constant across all turbines and inflow classes (i.e., $\iota^m_{\mathrm{az}} = \iota_{\mathrm{az}}$, $\mathcal{E}^m_{\mathrm{az}} = \mathcal{E}_{\mathrm{az}}$, etc.).

At any downstream position, the instantaneous total velocity deficit due to all upstream turbines can be expressed as

$$\Delta\Xi_{\mathrm{tot}}(x,y,z,t) = \mathcal{Q}\Big(\{\Delta\Xi^m(x,y,z,t)\}_{m\in\hat{\mathcal{M}}(x,y,z)} \Big), \tag{5}$$

where $\hat{\mathcal{M}}(x,y,z)$ denotes the set of upstream turbines influencing that location, and $\mathcal{Q}(\cdot)$ represents the superposition operator consistent with the FAST.Farm merging rule.

The inflow is generated using TurbSim, configured for IEC Class-C turbulence under neutral atmospheric stratification. Ten-minute full-field stochastic wind samples are provided as input to FAST.Farm, ensuring consistent turbulent inflow, wake dynamics, and rotor-averaged load predictions across all turbines.

By embedding the dynamic wake meandering formulation within the aeroelastic loop and driving it with realistic turbulent inflow, this model enables (i) evaluation of controller-induced transient responses under evolving wakes, (ii) quantification of incremental fatigue damage caused by wake-added turbulence in multi-wake interactions, and (iii) scalable probabilistic lifetime assessment across the wind farm.

2.3. Structural integrity model

This section outlines the methods used to evaluate the structural integrity and reliability of wind turbine support structures. Two complementary models are employed: a crack propagation model, which facilitates condition monitoring by simulating fatigue-induced crack growth, and a Failure Assessment Diagram (FAD) model, which enables criticality assessment through fracture mechanics-based evaluation. The combined use of these models supports both damage prognosis and safety evaluation.

2.3.1. Crack propagation model

To enable condition assessment of wind turbine support structures with respect to fatigue, a fracture mechanics-based simulation of crack propagation is employed. In this study, crack depth is used as the structural condition indicator. Considering an elliptical crack shape and assuming a fixed crack aspect ratio, the propagation of crack depth can be described by the relationship between the crack growth rate (da/dN) and the stress intensity factor range (ΔK) [104]:

$$\frac{da}{dN} = C(\Delta K)^{\widetilde{m}_{\mathrm{c}}} \tag{6}$$

in which a is the crack depth, ΔK is the stress intensity factor range, C and $\widetilde{m}_{\mathrm{c}}$ are the crack growth parameters and da/dN is the crack growth rate with respect to the number of cycle (N). ΔK_{th} is the threshold stress intensity factor range. $da/dN = 0$ if $\Delta K < \Delta K_{\mathrm{th}}$. In this study, a critical crack depth threshold (a_L) is defined to represent the onset of failure. Additionally, the effect of crack closure is ignored in the crack propagation simulation. The stress intensity factor is used to predict the stress state near the tip of a crack or notch caused by a remote load and plays a vital role in the application of linear elastic fracture mechanics [105]. The general form of stress intensity factor solution reads as follows:

$$K = (Y\sigma)\sqrt{\pi a} \tag{7}$$

where σ is the remote stress acting on the structural member and Y is the geometry function, which is assumed to take the value of one for simplicity. For fatigue analysis, the corresponding stress intensity factor range is given as:

$$\Delta K = (Y\Delta\sigma)\sqrt{\pi a} \tag{8}$$

An incremental approach is applied to simulate the crack propagation in the cycle i, in which if $\Delta K > \Delta K_{\mathrm{th}}$ the crack growth increment is estimated as follows:

$$\Delta a_i = C(\Delta K)^{\widetilde{m}_{\mathrm{c}}}\Delta N \tag{9}$$

The cumulative crack depth after N cycles is then obtained as follows:

$$a_N = a_0 + \sum_{i=1}^{N} \Delta a_i \tag{10}$$

In this study, multiple load cases are considered as described in Section 2.2, each defined by different combinations of wind direction

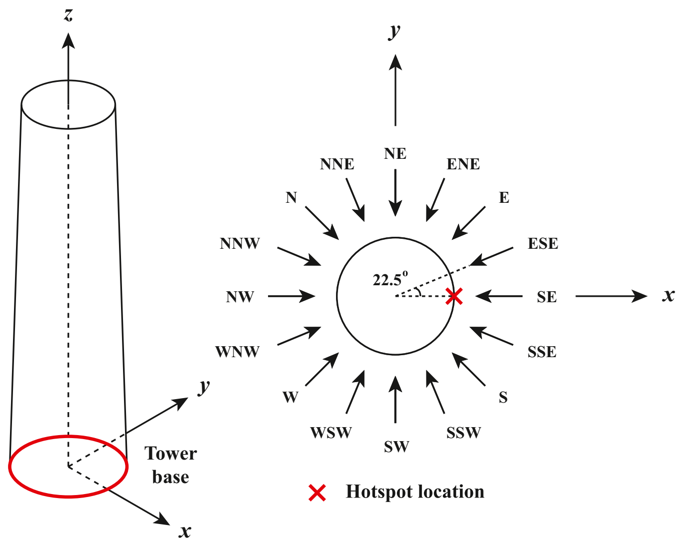

Fig. 2. Illustration of the selected hotspot location.

and wind speed, as detailed in the previous section. The time histories of the tower base fore–aft bending moment obtained for each load case are first used to calculate the corresponding nominal stress histories at a selected hotspot on the tower base cross-section, based on the corresponding cross-sectional properties (Fig. 2). This hotspot is selected because it represents the most highly stressed region under the fore–aft bending moment, which is the only environmental load effect considered in this study. Consequently, it is regarded as the most critical location for fatigue crack growth and structural integrity assessment. It should be noted that other locations may become critical when additional load effects or alternative loading scenarios are considered. However, the proposed framework is not restricted to a single hotspot and can be readily extended to multiple critical locations. The stress history obtained for each load case is then used to derive an equivalent constant-amplitude stress range, denoted as $\Delta\sigma_{\mathrm{eq},i}$. This is calculated using a weighted averaging approach expressed as:

$$\Delta\sigma_{\mathrm{eq},i} = \left[\int_0^{\infty} \Delta\sigma^{\beta} f(\Delta\sigma) d\Delta\sigma\right]^{1/\beta} \tag{11}$$

where $\Delta\sigma_{\mathrm{eq},i}$ is the equivalent constant-amplitude stress range for load case i, and $f(\Delta\sigma)$ denotes the probability distribution of stress range. In practice, rainflow counting is applied to the variable-amplitude stress histories to generate the stress range histograms. The parameter β is a material-specific exponent, typically corresponding to the slope of the fatigue crack growth curve in log–log space. Once the equivalent constant-amplitude stress ranges are obtained for all load cases, an overall equivalent stress range across all load cases is computed as:

$$\Delta\sigma_{\mathrm{eq}} = \left[\sum_{i\in\mathcal{I}} \left(\Delta\sigma_{\mathrm{eq},i}\right)^{\beta} \cdot p_i\right]^{1/\beta} \tag{12}$$

where p_i is the probability of occurrence of load case i and $\mathcal{I}$ is the total number of load cases. It should be noted that not all load cases generate a tensile stress history at the selected hotspot. For such cases, their contribution to the equivalent stress range is excluded by setting the corresponding probability of occurrence to zero. To account for local stress concentration, a stress concentration factor (SCF) is applied to the nominal stress range obtained by Eq. (12) prior to use in the crack-propagation analysis. This simplification is adopted to maintain the tractability of the integrated framework and to keep the focus on how wake-induced loading differences propagate into structural degradation and maintenance decision-making, rather than on detailed local finite-element stress modeling. Accordingly, the resulting stress and crack-growth estimates should be interpreted mainly as comparative indicators among turbines under consistent modeling assumptions, rather than as final design-level hotspot stress predictions. Within the scope of the present framework demonstration, advanced local stress analysis is therefore not pursued. In future studies, more comprehensive stress analysis could be incorporated to facilitate hotspot identification and support more rigorous structural integrity assessment.

2.3.2. Crack acceptability and structural reliability assessment

According to BS 7910 [62], for cracked structures, failure typically occurs through fracture, plastic collapse, or a combination of both. The ECA methodology, based on the FAD, is specifically developed to evaluate the interaction between these two failure modes and to assess the acceptability of cracks. Within this framework, two main parameters are required, namely load ratio (L_r) and fracture ratio (K_r). The load ratio (L_r) is determined from the primary load (P) acting on the structure:

$$L_r = \frac{P}{P_L(a, \sigma_Y)} = \frac{\sigma_{\mathrm{ref}}}{\sigma_Y} \tag{13}$$

where $P_L(a, \sigma_Y)$ is the elastic-perfectly plastic limit load for crack depth a and yield strength σ_Y. σ_{ref} is the reference stress acting on the structure, computed from the applied membrane stress (σ_m) and the crack depth.

With respect to the fracture ratio (K_r), it is determined by the following equation:

$$K_r = \frac{K^{\mathrm{P}} + V K^{\mathrm{S}}}{K_{\mathrm{mat}}} \tag{14}$$

where K^{P} is the stress intensity factor due to primary stress (i.e., σ_{ref} in Eq. (13)), K^{S} is the stress intensity factor due to secondary stress (σ_S), and K_{mat} is the material's fracture toughness.

The term V is the plasticity correction factor and is expressed as follows:

$$V = \min\left[1 + 0.2L_r + 0.02K^{\mathrm{S}}\left(\frac{L_r}{K^{\mathrm{P}}}\right)(1+2L_r),\ 3.1 - 2L_r\right] \quad \text{for} \quad L_r \le 1.05 \tag{15}$$

$$V = 0.4 \quad \text{for} \quad L_r > 1.05 \tag{16}$$

The assessment point is evaluated against the Failure Assessment Line (FAL), which, together with the coordinate axes, defines a safe domain. If the point lies within this domain, the structure is considered safe and the crack deemed acceptable (Fig. 3):

$$\Psi_{\mathrm{safe}} = \left\{(L_r, K_r) \in \mathbb{R}^2 : 0 \le L_r \le L_{r,\max},\ 0 \le K_r \le f(L_r)\right\} \tag{17}$$

where the function $f(\cdot)$ is the formulation of FAL. The Option 1 procedure described by BS 7910 is employed in this work. For materials exhibiting a yield discontinuity such as offshore steel considered in the present work, the following equations are used to describe the FAL:

$$f(L_r) = \left(1 + \frac{1}{2}L_r^2\right)^{-0.5} \quad \text{for} \quad L_r < 1 \tag{18}$$

$$f(L_r) = \left(\lambda + \frac{1}{2\lambda}\right)^{-0.5} \quad \text{for} \quad L_r = 1 \tag{19}$$

$$f(L_r) = f(L_r = 1) \cdot L_r^{(M-1)/(2M)} \quad \text{for} \quad 1 < L_r < L_{r,\max} \tag{20}$$

$$f(L_r) = 0 \quad \text{for} \quad L_r \ge L_{r,\max} \tag{21}$$

in which the parameter M is given as a function of material yield strength (σ_Y) and ultimate tensile strength (σ_U) as follows:

$$M = 0.3\left(1 - \frac{\sigma_Y}{\sigma_U}\right) \tag{22}$$

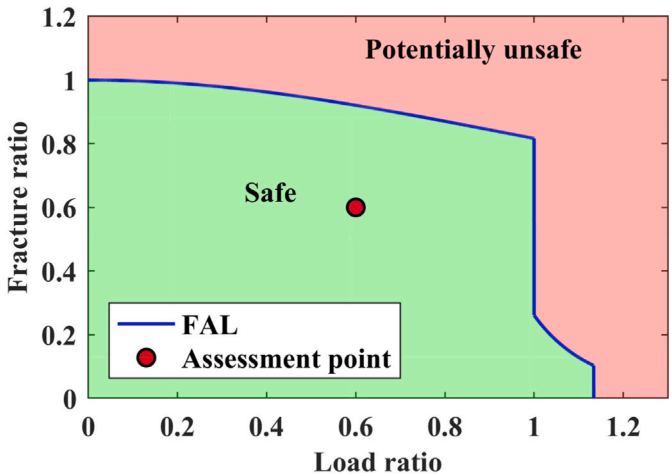

Fig. 3. Illustration of failure assessment diagram.

Additionally, $L_{r,max}$ denotes the cut-off value of FAL and is determined by the following solution:

$$L_{r,max} = \frac{\sigma_Y + \sigma_U}{2\sigma_Y} \tag{23}$$

Furthermore, the parameter λ is defined in terms of elastic modulus (E), the yield strength (σ_Y), and the increase in strain ($\Delta\varepsilon$) at lower yield strength:

$$\lambda = 1 + \frac{E\Delta\varepsilon}{\sigma_Y} \tag{24}$$

in which

$$\Delta\varepsilon = 0.0375(1 - 0.001\sigma_Y) \tag{25}$$

Additionally, to account for the inherent uncertainties in input variables, a probabilistic ECA is performed. Specifically, a Monte Carlo simulation is employed to estimate the probability of failure ($P_{failure}$) and structural reliability ($R = 1 - P_{failure}$). For each sampled set of inputs, an assessment point ($L_r^{(l)}, K_r^{(l)}$) is computed and checked against the safe domain (Ψ_{safe}). An indicator function is defined to denote whether the structure is safe under the l-th ($l \in \mathcal{L}$) sample:

$$I_{safe}^{(l)} = \begin{cases} 1, & \text{if } (L_r^{(l)}, K_r^{(l)}) \in \Psi_{safe} \quad \text{(safe)} \\ 0, & \text{otherwise} \quad \text{(failure)} \end{cases} \tag{26}$$

The probability of failure is then approximated by:

$$P_{failure} \approx \frac{1}{\mathcal{L}} \sum_{l=1}^{\mathcal{L}} \left(1 - I_{safe}^{(l)}\right) \tag{27}$$

Material yield strength (mean = 355 MPa, CoV = 10%), ultimate tensile strength (mean = 550 MPa, CoV = 10%), fracture toughness (mean = 150 MPa$\sqrt{m}$, CoV = 10%), applied membrane stress (mean = 250 MPa, CoV = 20%), and crack size (mean value obtained from the crack propagation simulation, CoV = 20%) are considered as random variables in the probabilistic ECA. For simplicity and in accordance with the recommendations of BS 7910, all variables are assumed to follow normal distributions. To improve computational efficiency, a sample size of 10,000 is adopted based on a sensitivity study using 10,000, 50,000, and 100,000 samples, which showed reasonably small differences in the predicted probabilities of failure.

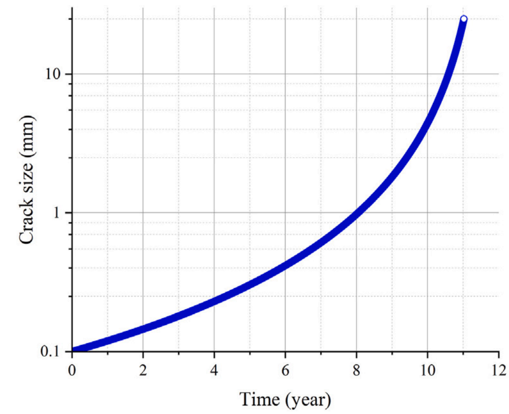

Fig. 4. Illustration of crack propagation over time.

2.4. Operation and maintenance optimization model

2.4.1. Condition-based opportunistic maintenance strategy

The outputs from the structural integrity model provide the direct inputs to the O&M decision-making model. Specifically, the turbine-specific crack depth trajectories are used as condition states for inspection and maintenance threshold comparison, while the corresponding reliability estimates are used to evaluate the reliability objective in the optimization model. Suppose that the offshore wind farm consists of $\mathcal{M}$ wind turbines. Although all wind turbine towers are assumed to be in brand-new condition at the start of farm operation, micro-scale initial cracks may still exist due to inherent imperfections introduced during the manufacturing and welding processes. Therefore, an initial crack depth is denoted as a_{IN}. For the wind turbine m ($m = 1, 2, \ldots, \mathcal{M}$), let a_j^m represent the crack size observed on the tower of turbine m during the j-th inspection with the total number of inspections denoted by $\mathcal{J}$.

Fig. 4 illustrates a trajectory of crack propagation over time. Due to the inherent characteristics of crack growth in tower structures, the initial propagation is relatively slow. Crack growth is limited during the initial years, but as depth accumulates, the growth rate accelerates markedly.

The cracks in turbine towers are inspected at regular intervals using remote inspection and advanced SHM technologies. In practice, however, the condition of offshore assets is rarely fully observable. Since the primary objective of this study is to investigate wind-farm heterogeneity and quantify the long-term implications of wake effects, a fully effective inspection process is assumed for model tractability. This idealized assumption is adopted to isolate the influence of wake-induced degradation heterogeneity on maintenance decision-making, without introducing additional uncertainties from imperfect detection, sizing errors, or inspection delays. Accordingly, the inspection model should be interpreted as an ideal information-availability case, while imperfect inspection can be incorporated in future extensions of the framework. Specifically, the adopted inspection techniques are assumed capable of identifying the actual size of fatigue cracks within a relatively short period after inspection. The inspection interval is denoted by the variable ζ.

If the crack reaches a predefined critical depth denoted by a_L, the tower is considered to be at high risk of collapse. In such cases, a complete replacement of the tower is required. This type of maintenance is referred to as corrective replacement, which typically incurs the highest maintenance cost and results in significant downtime. The corrective replacement triggers a maintenance cycle, denoted by s, which involves organizing and dispatching available vessels and maintenance crews to maintain the wind turbines that meet the maintenance criteria.

To avoid such costly corrective actions, the condition-based opportunistic maintenance strategy is introduced based on the intermediate maintenance threshold φ_p. The threshold is compared with the observed crack size a_j^m to determine whether a maintenance cycle is triggered preventively. If the crack depth exceeds the threshold ($\varphi_\mathrm{p} \le a_j^m < a_\mathrm{L}$), a preventive maintenance is planned and a maintenance cycle is initiated.

In each maintenance cycle, when a turbine with a crack depth exceeding the critical threshold a_L is replaced, or when preventive maintenance is performed on a turbine exceeding the threshold φ_p, maintenance opportunities may arise for other turbines within the wind farm. Specifically, an additional maintenance threshold φ_o is introduced and compared with the current crack depth a_j^m to determine whether opportunistic maintenance should be carried out. If the condition $\varphi_\mathrm{o} \le a_j^m < \varphi_\mathrm{p}$ is satisfied, the turbine is scheduled for opportunistic maintenance.

Two methods are considered for tower repair in this study. The first is grinding, which is used to remove minor surface cracks [88]. In the proposed model, this method is employed for opportunistic maintenance. Since the crack depth at this stage is relatively small and the repair procedure is relatively simple, the associated maintenance cost is lower. The second method is welding, which targets deeper cracks [70]. It involves grinding to eliminate the surface crack area, followed by wet welding to fill the resulting groove. In the model, this procedure is used to perform preventive maintenance.

When performing maintenance on a repairable system such as wind turbine structures, it is necessary to model the effect of maintenance actions on the accumulated crack depth. In this study, we adopt the Kijima II model, which assumes that the maintenance action in the s-th maintenance cycle can reduce the cumulative damage (i.e., crack growth) accumulated up to that point. This relationship can be expressed as [106]:

$$a_{j_s}^m = g\left(\mathcal{T}_{j_s}^m\right) = g\left(q \cdot \left(\mathcal{T}_{j_{(s-1)}}^m + t_s - t_{(s-1)}\right)\right) \tag{28}$$

where the function $g(\cdot)$ serves as a mapping from the virtual age to the current crack level, $a_{j_s}^m$ represents the crack depth observed on turbine m at the s-th maintenance cycle which is triggered by the j_s-th inspection, $\mathcal{T}_{j_s}^m$ represents the corresponding virtual age, q is repair effectiveness, and t_s and $t_{(s-1)}$ represent the time of s-th and $(s-1)$-th maintenance cycles. The total number of maintenance cycles is denoted as $\mathcal{S}$. In this case, the value of q is set to 0. This full-restoration assumption represents an ideal repair case and is adopted to avoid introducing additional uncertainty associated with repair quality and residual defects. Under this assumption, the post-maintenance crack state is reset to the initial condition. In practice, imperfect repair effects can be represented by assigning a non-zero repair effectiveness parameter in the Kijima model, implying that all types of maintenance are assumed to fully restore the crack to its initial state upon execution.

Fig. 5 is presented to illustrate the proposed maintenance strategy. Suppose three wind turbines begin with initial crack depth denoted by a_IN. The crack propagation is monitored at inspection points spaced at intervals of ζ, from t_1 to t_6. At time t_1, all crack depths are below the opportunistic maintenance threshold φ_o, and therefore, no maintenance cycle is triggered. At t_2, wind turbine 2 reaches the preventive maintenance threshold φ_p and is scheduled for preventive maintenance, initiating a maintenance cycle. The other turbines remain below φ_o, and thus are not eligible for maintenance at this time. At t_3, the crack in wind turbine 1 grows rapidly and reaches the critical threshold a_L, requiring corrective replacement. This maintenance cycle also creates an opportunity to perform opportunistic maintenance on wind turbine 3, which now satisfies $\varphi_\mathrm{o} \le a_j^3 < \varphi_\mathrm{p}$. The scenario at t_4 is similar to that at t_2, where only wind turbine 2 qualifies for preventive maintenance. At t_5, the situation resembles that of t_1, with no turbines meeting any maintenance criteria. Finally, at t_6, the corrective replacement of wind turbine 1 and the preventive maintenance of wind turbine 2 jointly provide a maintenance opportunity to perform opportunistic maintenance on wind turbine 3.

2.4.2. Cost and reliability objective formulation

The proposed maintenance strategy considers two key performance indicators as optimization objectives, i.e., minimizing O&M costs and maximizing reliability. The O&M costs refer to the annual maintenance expenditure over the lifetime T_d of the offshore wind farm. The cost categories include repair costs, mobilization costs, inspection costs, and transportation costs. All the costs are discounted using a factor γ which is in the range $[0, 1]$ to account for the time value of money.

We define $\mathcal{H} = \{\mathrm{cm}, \mathrm{pm}, \mathrm{om}\}$ as the set of maintenance action types, where "cm", "pm", "om" represent corrective maintenance, preventive maintenance, and opportunistic maintenance, respectively. The total repair costs C_R are derived as

$$C_\mathrm{R} = \sum\nolimits_{s\in\mathcal{S}} \sum\nolimits_{m\in\mathcal{M}} \left(\sum\nolimits_{h\in\mathcal{H}} C_h^{s,m} y_h^{s,m}\right)\gamma^{t_s} \tag{29}$$

where $y_h^{s,m}$ is the binary variable denoting if a maintenance action is required for wind turbine m in the maintenance cycle s, $C_h^{s,m}$ is the cost for different types of maintenance, in which the costs for preventive maintenance and opportunistic maintenance are related to the crack depth.

$$C_\mathrm{pm}^{s,m} = (a_{j_s}^m - \varphi_\mathrm{p})C_\mathrm{pm}^\mathrm{UN} + (\varphi_\mathrm{p} - \varphi_\mathrm{o})C_\mathrm{om}^\mathrm{UN} + (\varphi_\mathrm{o} - a_\mathrm{IN})C^\mathrm{UN} \tag{30}$$

where $C_\mathrm{pm}^\mathrm{UN}$, $C_\mathrm{om}^\mathrm{UN}$, C^UN are the cost rate for repairing crack with depth higher than φ_p, between φ_o and φ_p, and below φ_o, respectively.

$$C_\mathrm{om}^{s,m} = (a_{j_s}^m - \varphi_\mathrm{o})C_\mathrm{om}^\mathrm{UN} + (\varphi_\mathrm{o} - a_\mathrm{IN})C^\mathrm{UN} \tag{31}$$

The mobilization costs C_M are estimated as

$$C_\mathrm{M} = \sum\nolimits_{s\in\mathcal{S}} C_\mathrm{mo}^s \gamma^{t_s} \tag{32}$$

where C_mo^s is the mobilization cost for maintenance cycle s.

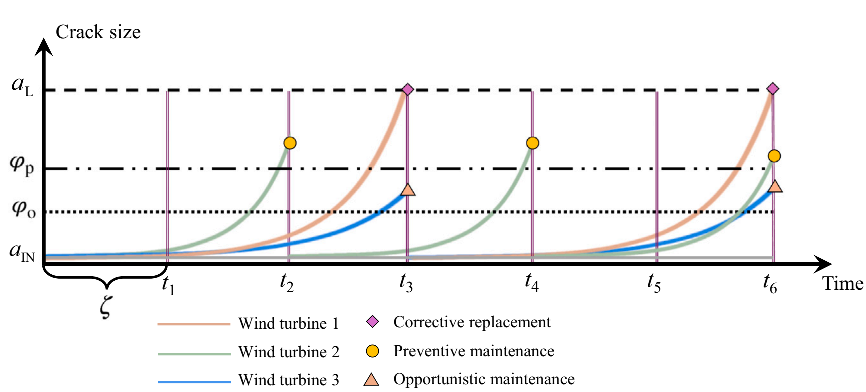

Fig. 5. Illustration of the proposed condition-based opportunistic maintenance strategy.

The total inspection costs C_I over the lifetime are calculated as

$$C_\mathrm{I} = \sum_{j\in\mathcal{J}} \sum_{m\in\mathcal{M}} C_\mathrm{in}^{j,m} \gamma^{t_j} \tag{33}$$

where $C_\mathrm{in}^{j,m}$ is the inspection cost for wind turbine m in the j-th inspection.

We use $\mathcal{U} = \{\mathrm{JV}, \mathrm{SV}, \mathrm{CV}\}$ as the set of maintenance service vessel types, where JV, SV, CV represent jack-up vessels, service operation vessels, and crew transfer vessels, respectively. These vessels are used to perform corrective maintenance, preventive maintenance, and opportunistic maintenance, respectively. The total transportation costs C_T are calculated as

$$C_\mathrm{T} = \sum_{s\in\mathcal{S}} \sum_{m\in\mathcal{M}} \left(\sum_{u\in\mathcal{U}} \left(C_u + \delta v_u\right) \omega_h y_h^{s,m} \right) \gamma^{t_s} \tag{34}$$

where C_u is the daily vessel cost, δ is daily personnel cost, v_u is the number of the required maintenance personnel, ω_h is the repair time.

Therefore, the annual O&M costs A_om are calculated as

$$A_\mathrm{om} = \frac{C_\mathrm{R} + C_\mathrm{M} + C_\mathrm{I} + C_\mathrm{T}}{T_\mathrm{d}} \tag{35}$$

Another optimization objective is the average reliability of the wind turbine throughout its lifetime. Reliability is directly correlated with crack depth. When the crack depth remains small, the reliability decreases slowly. However, once the crack exceeds a threshold, the reliability drops sharply. According to Eq. (27), the tower reliability for wind turbine m at j-th inspection, $R_\mathrm{y}(a_j^m)$, is estimated based on the corresponding failure probability. The average wind turbine reliability R_wt is derived by

$$R_\mathrm{wt} = \frac{\sum_{j\in\mathcal{J}} \sum_{m\in\mathcal{M}} R_\mathrm{y}(a_j^m)}{\mathcal{M}\mathcal{J}} \tag{36}$$

2.4.3. Optimization method

The section formulates the O&M optimization model and describes the process of searching for the optimal solutions among possible options. The decision vector of the optimization problem is:

$$\Omega = \left[\varphi_\mathrm{p}, \varphi_\mathrm{o}, \zeta\right] \tag{37}$$

The objective is to identify the optimal maintenance strategy which maximizes the wind turbine reliability while minimizing the O&M expenditure. The value of the optimal strategy Ω^* is described by the value function:

$$\Omega^* = \arg\min \left[A_\mathrm{om}(\Omega),\ -R_\mathrm{wt}(\Omega) \right] \tag{38}$$

Subject to:

$$a_\mathrm{L} \geq \varphi_\mathrm{p} > \varphi_\mathrm{o} \geq a_\mathrm{IN} \tag{39}$$

$$\zeta \in \mathbb{Z}^+ \tag{40}$$

$$\mathcal{S}, \mathcal{M}, \mathcal{J} \in \mathbb{Z}^+ \tag{41}$$

$$\zeta \mathcal{J} \leq T_\mathrm{d} \tag{42}$$

$$y_h^{s,m} \in \{0,1\} \quad \forall s \in \mathcal{S}, m \in \mathcal{M}, h \in \mathcal{H} \tag{43}$$

Constraint (39) restricts the logical relationship among the maintenance thresholds and ensures that the thresholds lie within the range between the initial and critical crack depths. Constraints (40) and (41) restrict the corresponding parameters to be positive integers. Constraint (42) ensures that the offshore wind farm lifetime fully covers inspection schedules. Constraint (43) guarantees that each maintenance decision is modeled as a binary variable.

The optimization problem involves nonlinearities, combinatorial relationships, and multiple objectives. Among existing approaches, the Non-dominated Sorting Genetic Algorithm II (NSGA-II) is one of the most widely used methods for multi-objective maintenance optimization [107]. Owing to its effectiveness and suitability for solving complex multi-objective problems [108], NSGA-II is adopted in this study as the optimization method. After initializing the ranges of decision variables and setting the parameters of the NSGA-II algorithm, an initial population is generated. Each individual in the population is evaluated by running the maintenance model to compute the two objective functions, $A_\mathrm{om}(\Omega)$ and $R_\mathrm{wt}(\Omega)$, and to determine whether the individual satisfies the given constraints. Subsequently, the population undergoes non-dominated sorting and crowding distance calculation. Then, the individuals are selected for crossover and mutation to generate offspring. The parent and offspring populations are then combined to form an intermediate population. Through elitism, the best individuals are preserved and selected to constitute the next generation. This process is iteratively repeated until a predefined termination criterion is met.

Table 1
Parameters for crack growth modeling.

	Symbol	Unit	Value
Crack growth coefficient	C	–	1.83×10^{-13}
Crack growth exponent	$\widetilde{m}_\mathrm{c}$	–	3
Initial crack depth	a_0	mm	0.1
Stress concentration factor	SCF	–	3.5

Table 2
Parameters for probabilistic engineering critical assessment.

	Symbol	Unit	Distribution	Mean	Coefficient of variation
Material yield strength	σ_Y	MPa	Normal	355	10%
Material ultimate tensile strength	σ_U	MPa	Normal	550	10%
Material fracture toughness	K_{mat}	MPa$\sqrt{m}$	Normal	150	10%
Membrane stress	σ_m	MPa	Normal	250	20%
Secondary stress	σ_S	MPa	Deterministic	100	–

3. Results and discussion

3.1. Scenario set-up

Japan's first commercial-scale offshore wind farm is located at the Akita Port and Noshiro Port, which has been in operation since January 2023 [109]. All turbines are bottom-fixed structures. The O&M base is situated at Noshiro Port, and the designed operational lifetime of the wind farm T_d is 20 years. The wind turbine tower is modeled following the specifications in [110], with a tapered geometry characterized by a base diameter of 6.0 m and thickness of 0.027 m, and a top diameter of 3.87 m and thickness of 0.019 m. The parameters used in structural integrity assessments are summarized in Tables 1 and 2.

For this case study, ten years of wind data for the coastal area at Akita, Japan (14 December 2014 - 13 December 2024) were collected directly from the NeoWins platform (Fig. 6) [111]. Because NeoWins provides only daily mean records, our dataset comprises 3653 entries of wind speed and corresponding wind direction classifications (each assigned to one of 16 compass sectors). To represent a small coastal wind farm, we overlay a virtual 3×3 turbine array on this site. The use of NeoWins' daily resolution data ensures that the simulation captures the region's prevailing wind condition characteristics while remaining computationally efficient.

Due to the current lack of offshore wind O&M data in Japan, most of the input O&M parameters in this study are referenced from wind energy datasets reported in Europe. The exchange rate is approximated as 1 $e \approx$ 168 ¥. Tables 3 and 4 list the key parameters for maintenance types and vessels [67,107,112–114]. Other parameter values are set as follows [60,

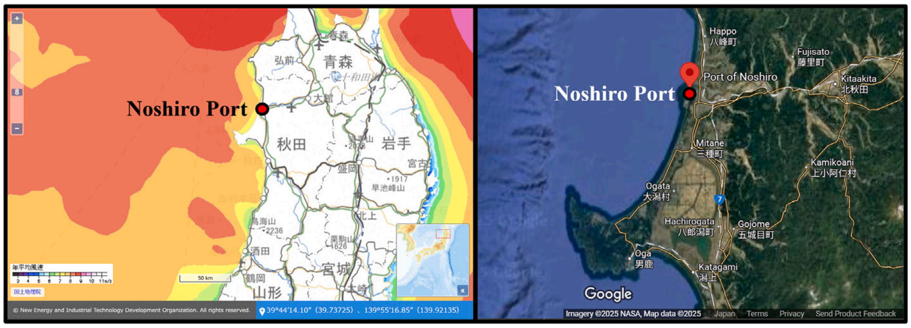

Fig. 6. Wind resource around Akita area in NeoWins platform [111] (left), close-up view of Noshiro port in Google Maps (right).

Table 3
Repair costs and times [67,112–115].

	Time (day)	Cost (k¥)
Corrective maintenance	10	184,800
Preventive maintenance	2	–
Opportunistic maintenance	1	–
Inspection	–	168

Table 4
Parameters for different types of vessels [107].

	Daily cost (k¥)	Number of technicians
Jack-up vessel	8400	20
Service operation vessel	3024	8
Crew transfer vessel	1344	4

Table 5
NSGA-II parameter setting.

NSGA-II parameter	Value/type
Maximum generation	100
Population size	100
Mutation probability	0.17
Crossover probability	0.67
Mutation operator	Gaussian mutation
Crossover operator	Intermediate crossover

67,112–117]: cost rates $C^{UN} = 168$ k¥/mm, $C^{UN}_{om} = 504$ k¥/mm, $C^{UN}_{pm} = 1008$ k¥/mm, annual discount factor is 0.98, maintenance effectiveness $q = 0$, critical crack depth $a_L = 25$mm, mobilization cost per maintenance round is 8400 k¥, and technician daily cost is 100.8 k¥. Table 5 lists the parameter settings for the NSGA-II optimization method.

3.2. Wind farm simulation results

3.2.1. Wind condition and wind farm configuration

Fig. 7 presents the wind rose at the study site, showing that the flow is predominantly from the southeast sector, with the highest frequency occurring at ESE (112.5°) and SE (135°), which together account for approximately 50% of all wind directions. Moderate winds (3–7 m/s) dominate across every direction but are particularly prevalent in the SE–ESE sector. Higher speeds (7–11 m/s) occur most often in the same southeast quadrant at roughly 5–10% frequency, while gusts exceeding 11 m/s are rare (< 5%), even in the principal wind sector. Winds from the opposite direction (NW) are sporadic and account for less than 10% of the record. Together, these data indicate a predominantly light-to-moderate southeast wind resource and suggest that turbine nacelles should be oriented toward the SE sector to maximize annual energy yield. The probability density function of wind speed at the study site (Fig. 8) exhibits a right-skewed, long-tailed distribution characterized by

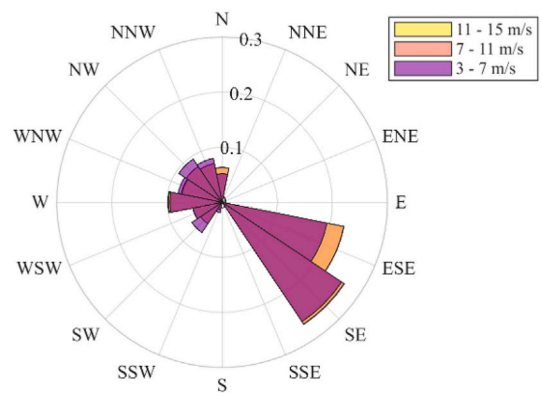

Fig. 7. Wind rose at Akita coastal area.

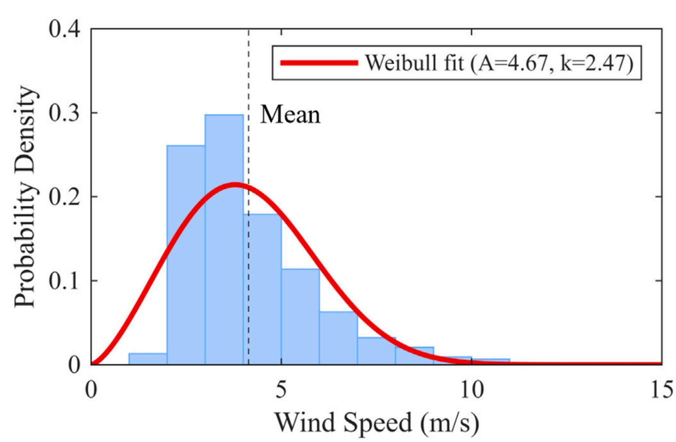

Fig. 8. Probability density function of wind speed at the study site with two-parameter Weibull fit.

a mean of approximately 4.1 m/s and a modal value in the 3–4 m/s range. Maximum-likelihood estimation yields a two-parameter Weibull fit with scale parameter 4.67 m/s and shape parameter 2.47, indicating a moderately peaked distribution that decays steadily toward higher speeds. Light-to-moderate winds (3–7 m/s) dominate the record, while stronger winds in excess of 10 m/s are rare. This behavior implies that the bulk of annual energy production will occur under 3–7 m/s conditions. Note that all wind speeds are daily averages, which smooth out short-term gusts and reduce the apparent frequency of high-speed events. This simplification lowers computational complexity and provides a consistent benchmark for evaluating the model proposed in this paper. The annual distribution of daily averaged wind speed was used to characterize the

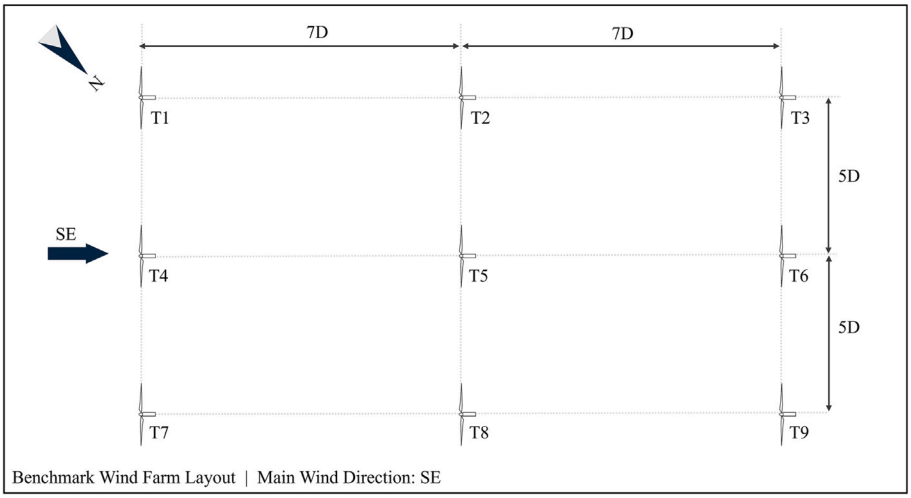

Fig. 9. Benchmark 3 × 3 wind farm layout with 7D longitudinal and 5D lateral spacing under prevailing SE wind direction.

Table 6
Wind farm configuration.

Wind farm parameter	Value/type
Wind turbine	NREL 5 MW Reference Wind Turbine
Wind farm layout	3 × 3 (L:14D W:10D)
Turbine distance	L:7D, W:5D
Wind farm orientation	SE

long-term wind climate and to identify representative mean wind-speed bins. It should be noted that the daily averaged wind speed was not used as the turbulent inflow time series for the fatigue simulations. Instead, for each representative wind-speed bin, a 10 min turbulent inflow field was generated independently using the prescribed bin-averaged mean wind speed and the corresponding turbulence parameters. In this way, the daily averaged wind-speed distribution was used only to provide the long-term occurrence probability of different mean wind-speed conditions, while the short-term turbulent fluctuations relevant to fatigue loading were explicitly represented in the subsequent 10 min turbulent inflow simulations.

The benchmark wind farm is arranged as a 3 × 3 rectangular grid of turbines (T1–T9), with three rows aligned in the main wind direction (SE) and three columns perpendicular to it (Fig. 9). Longitudinal spacing along SE is set to 7D to allow wake recovery under the dominant southeast winds, while lateral spacing of 5D limits wake overlap during side-winds. This configuration maximizes exposure of upstream machines (T1–T3) to free stream flow and maintains acceptable inter-row interference for oblique directions (e.g., ENE, SSE). Moreover, when winds come from ESE, the 7D×5D offset causes downstream turbines to lie outside the core wake of their upstream neighbors, thereby increasing incoming wind speed, boosting power production, and reducing turbulence-induced fatigue loads on blades and towers. For the wind turbine model, the NREL 5 MW reference wind turbine was selected in this study as described in Table 6.

Fig. 10 shows the wind speed distribution for each of the 16 wind direction sectors. In most sectors (e.g., N, ENE, E, S), wind speeds are almost exclusively in the below-rated band (3–7 m/s, represented by the 5 m/s bin), with vanishing or zero probability at 9 m/s and 13 m/s. Only a handful of sectors, most notably ESE and SW, exhibit small but non-negligible contributions at 9 m/s, and even fewer (W and WNW) at 13 m/s. By multiplying these directional occurrences by the three wind speed bin probabilities, a full 16 × 3 JPD matrix was constructed and zero-probability entries were discarded, yielding 27 unique inflow conditions as shown in Table 7. This discretization was adopted to balance computational cost and the need to represent the main wind climate and turbine operating conditions. The 16 wind-direction sectors capture the dominant directional variability of the site, while the three wind-speed bins represent the below-rated, around-rated, and above-rated operating regimes, which have distinct load-response characteristics. Since the long-term fatigue damage was calculated by weighting the fatigue contribution of each inflow condition using its occurrence probability in the JPD, this resolution was considered adequate for a representative life-cycle fatigue assessment. Nevertheless, a finer discretization of wind speed and wind direction may further improve the accuracy of site-specific lifetime fatigue estimation and will be investigated in future work.

Based on the 27 inflow conditions derived above, aeroelastic simulations were carried out in FAST.Farm. For each of the three representative wind speeds (5, 9, and 13 m/s), turbulent flow fields were generated with TurbSim [118] using the IEC NTM model with Category C turbulence. To cover all wind direction sectors without regenerating distinct three-dimensional flow fields for each wind direction, a single turbulence file per wind speed was employed, and the entire wind farm layout was rotated about the turbine hub coordinates by the required wind direction. By this method, consistent turbulence statistics were maintained across all 27 FAST.Farm cases, directional variability was efficiently captured via coordinate rotation, and JPD-based probability weights were incorporated.

3.2.2. Turbine loading and performance under wake

The comparison between the wake-affected and ideal no-wake cases shows that wake effects significantly influence both wind farm energy production and structural fatigue as described in Table 8. In the ideal no-wake case, the annual energy production (AEP) is 40.810 GWh/year, whereas in the wake-affected case it decreases to 32.296 GWh/year. This corresponds to a reduction of 8.514 GWh/year, or 20.863%, indicating that neglecting wake effects would clearly overestimate the farm's power output.

Wake effects also lead to a notable increase in fatigue loading. The annual cumulative fatigue damage rises from 6.347×10^{7} year^{-1} in the no-wake case to 9.377×10^{7} year^{-1} when wake effects are included, representing an increase of 47.724%. This increase is much larger than the relative AEP loss, suggesting that wake effects have an even stronger impact on structural loading than on power generation. Overall, wake effects impose a dual penalty on the wind farm by reducing energy production and increasing fatigue damage. Although the present fatigue-life-related values are mainly suitable for relative comparison, the results

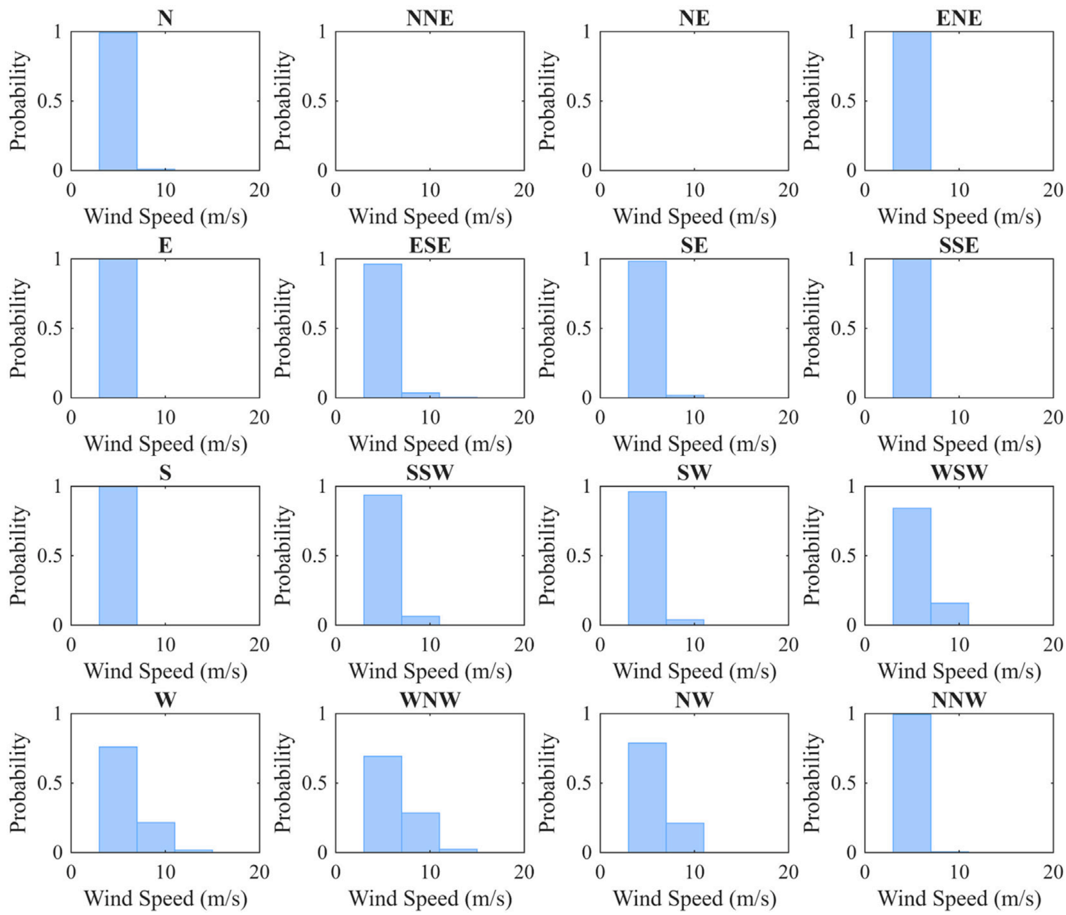

Fig. 10. Wind speed distributions across 16 wind direction sectors.

Table 7
Wind speed–direction joint probability density.

Wind direction	Below-rated region (5 m/s)	Around-rated region (9 m/s)	Above-rated region (13 m/s)
N	0.062378	0.000567	0.000000
NNE	0.000000	0.000000	0.000000
NE	0.000000	0.000000	0.000000
ENE	0.000547	0.000000	0.000000
E	0.003284	0.000000	0.000000
ESE	0.216147	0.007864	0.000674
SE	0.260950	0.004513	0.000000
SSE	0.000547	0.000000	0.000000
S	0.000547	0.000000	0.000000
SSW	0.012808	0.000876	0.000000
SW	0.044973	0.001825	0.000000
WSW	0.045111	0.008475	0.000000
W	0.074986	0.021241	0.002569
WNW	0.052724	0.021607	0.001750
NW	0.061461	0.016535	0.000000
NNW	0.071272	0.000430	0.000000

Table 8
Comparison of AEP and annual cumulative fatigue damage between no-wake and wake-affected cases.

Case	AEP (GWh /year)	AEP change (%)	Cumulative fatigue damage (year^{-1})	Fatigue damage change (%)
No wake	40.810	–	6.347×10^7	–
With wake	32.296	-20.863	9.377×10^7	$+47.724$

clearly show that ignoring wake effects would underestimate structural fatigue while overestimating annual energy yield.

Fig. 11 presents the wind farm flow fields under a mean inflow wind speed of 9 m/s for three representative wind directions. For inflow from the southeast (left panel) and southwest (right panel), the wakes generated by the upstream turbines extend downstream, causing substantial velocity deficits for most of the turbines located behind them. In particular, for the southwest direction, the shorter turbine spacing means that the wakes from the upstream turbines have insufficient distance to recover before impinging on the downstream rotors. Under such conditions, wake interactions are pronounced, with multiple downstream turbines located within overlapping wake regions, resulting in broader and more persistent low-speed zones. However, given the relatively low probability of occurrence of SW direction, its contribution to the overall accumulated fatigue loading of the turbines is comparatively small. In contrast, for the ESE (mid panel) direction, the turbine wakes are staggered relative to the downstream turbines, so that most downstream turbines are positioned outside the direct wake zones of the upstream units. This configuration substantially reduces both the extent and severity of velocity deficits, allowing higher inflow speeds at the downstream rotors and avoiding additional turbulence. Consequently, power losses and fatigue loads are both reduced in this wind direction.

To investigate the loading conditions of wind turbines in the wind farm for different wind directions, turbines enclosed by the red box (T4, T5, and T6) and the blue box (T2, T5, and T8) were selected for further analysis. All evaluation metrics were normalized with respect to the maximum value observed across the three wind turbines and the three wind directions.

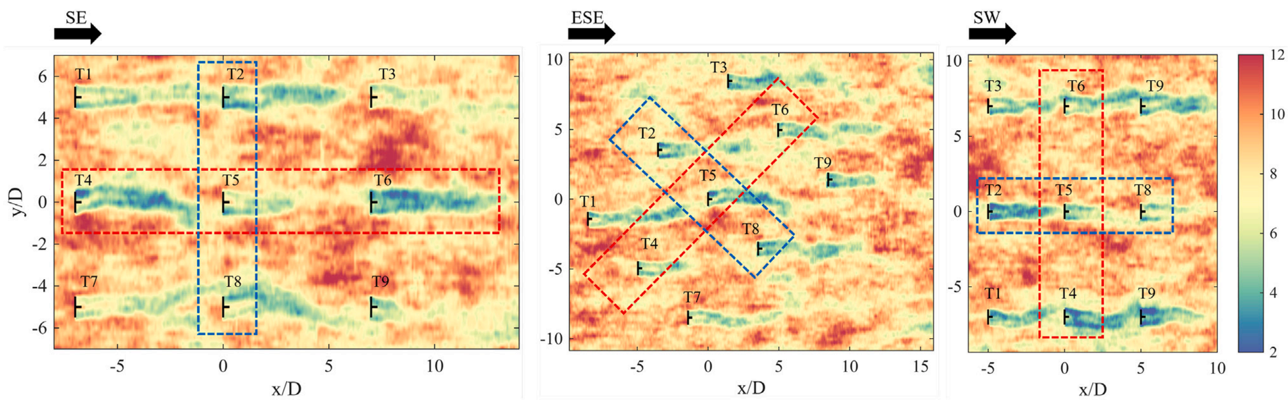

Fig. 11. Instantaneous wake flow field of wind farm for an incoming wind direction of SE, ESE and SW for wind speed of 9 m/s, wind turbines enclosed by red box (T4, T5 and T6) and blue box (T2, T5 and T8) are selected for loading analysis.

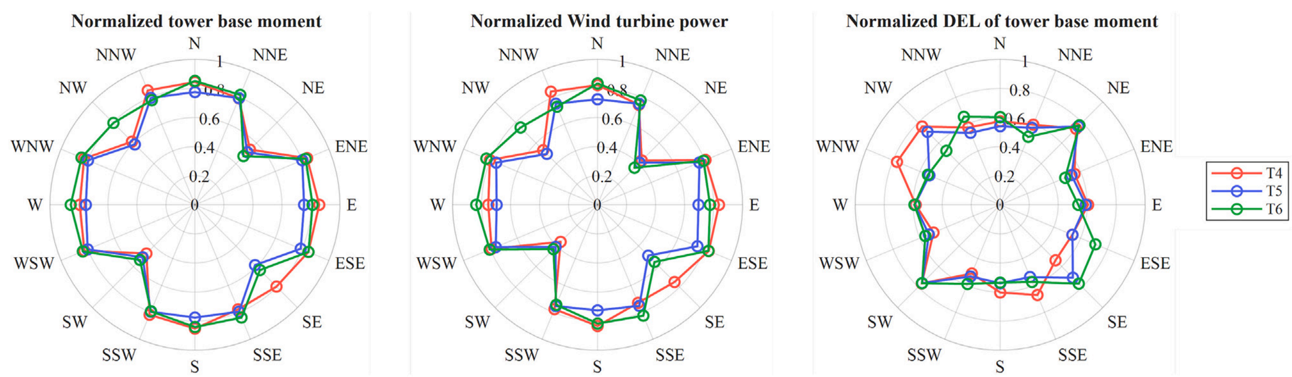

Fig. 12. Normalized statistical results of wind turbine base moment, power production and tower base DEL for wind turbines T4, T5 and T6.

The spatial distribution of wakes under different wind directions (Fig. 11) provides a physical basis for interpreting the observed variations in structural loading and power production. For inflow from the SE direction, the upstream turbine T4 generates a wake that extends directly toward T5 and T6, causing substantial velocity deficits and increased turbulence intensity in the downstream flow. These velocity deficits have a dual effect on fatigue loading: first, by increasing the added turbulence intensity, and second, by reducing the rotor speed such that the blade passing frequency approaches the first natural frequency of the tower, which can amplify structural response and accelerate fatigue damage [41]. This is reflected in the tower base moment results (Fig. 12), where T4 exhibits values approximately 20% higher than T5 and T6 in terms of instantaneous loading. However, when considering the DEL, T5 and T6 show significantly higher values, demonstrating that the combined effects of wake-induced turbulence and frequency proximity contribute substantially to long-term fatigue loading.

A similar pattern is observed for power production, with the downstream turbines experiencing reduced output due to wake deficits. In the ESE direction, the lateral shift of the wake results in partial flow recovery for T5, increasing the inflow wind speed and reducing its fatigue loading to a level comparable with T4. For T6, however, more complex wake interactions, originating from both T2 and T3, lead to a smaller reduction in fatigue loading, which nevertheless remains relatively high despite improved inflow conditions. When the inflow shifts to the SW direction, T4, T5, and T6 are positioned at the same downstream distance from the inflow, resulting in nearly identical fatigue loading and power output, as expected from the symmetric exposure to upstream wakes.

In contrast, the situation is reversed for turbines T2, T5, and T8 (blue box). For the SW direction, the downstream turbines T5 and T8 experience increased fatigue loading due to the wakes from their respective upstream turbines as shown in Fig. 13. The effect is amplified by the shorter turbine spacing, reduced from 7D to 5D, which limits wake recovery and intensifies turbulence. Consequently, fatigue loading increases more sharply, and power production decreases more rapidly compared with the red-box turbine group. This comparison highlights the combined influence of wake alignment, turbine spacing, and wind direction on both energy yield and structural fatigue in wind farms.

Figs. 14 and 15 present the weighted tower base moments, power production, and tower base DEL, where each wind direction is weighted by its probability of occurrence and normalized by the no-wake reference turbine. In the dominant SE wind direction, the influence of turbine wakes becomes even more pronounced when long-term directional occurrence is taken into account. The persistent exposure of downstream turbines such as T5 and T6 to the wake of their upstream neighbors leads to a further reduction in power output and a marked increase in lifetime fatigue loading. This amplified contribution demonstrates that frequent but moderate wake deficits can dominate long-term structural damage accumulation.

For the second most frequent direction, ESE, the lateral displacement of the wake substantially mitigates its impact. As the downstream turbines move partially outside the high-deficit wake core, both the DEL and power loss are significantly reduced for T5 and T6. The weighted results therefore highlight the strong dependence of long-term turbine performance on wake alignment and the prevailing wind-direction distribution.

Overall, these findings underscore the importance of wake-control strategies, such as wake steering or active yaw misalignment, in improving wind-farm-level efficiency. By reducing wake overlap in dominant

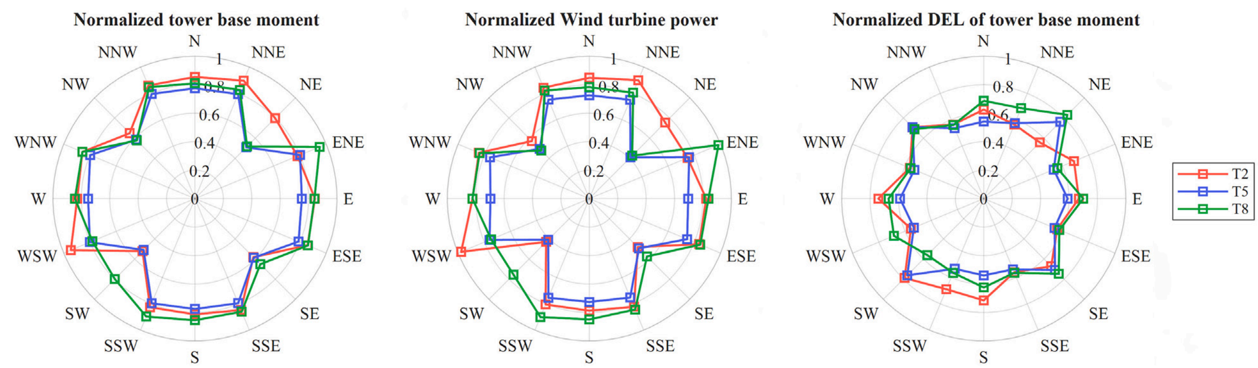

Fig. 13. Normalized statistical results of wind turbine base moment, power production and tower base DEL for wind turbines T2, T5 and T8.

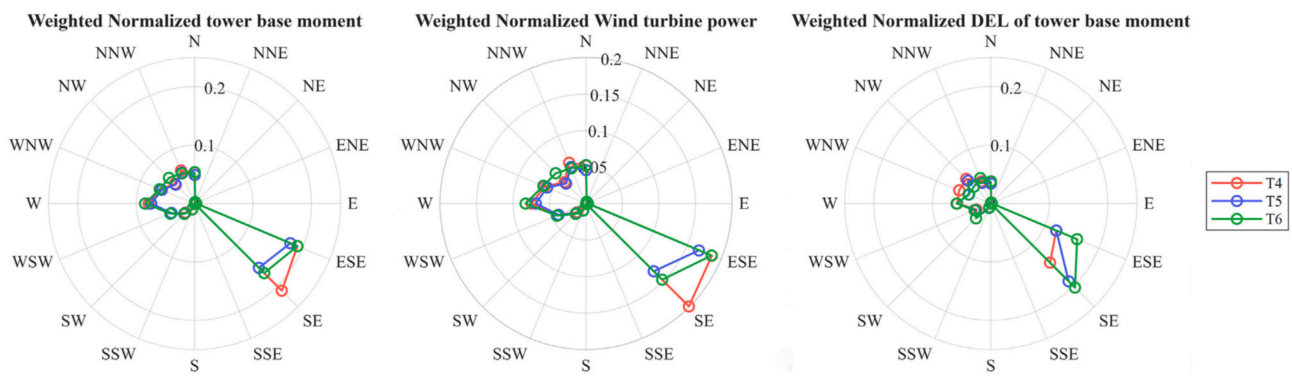

Fig. 14. Weighted normalized statistical results of wind turbine base moment, power production and tower base DEL for wind turbines T4, T5 and T6.

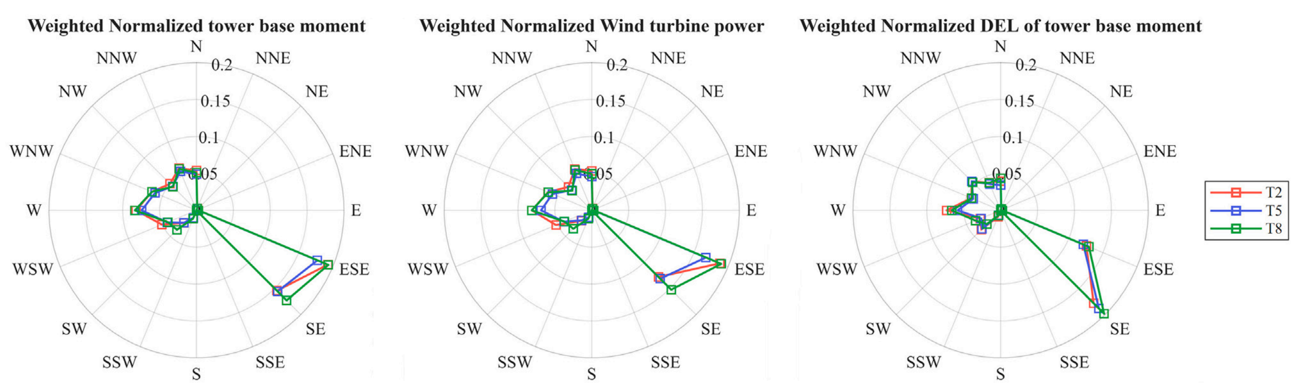

Fig. 15. Weighted normalized statistical results of wind turbine base moment, power production and tower base DEL for wind turbines T2, T5 and T8.

inflow sectors, such control approaches have the potential to simultaneously enhance energy yield and mitigate accumulated fatigue loads.

For turbines T2, T5, and T8, the weighted results in the dominant SE direction indicate that their wake-influenced operating conditions are largely similar. As a consequence, the differences in power production primarily arise from subtle variations in the inflow field rather than from fundamentally different wake exposure, and their DEL values remain nearly identical. This behavior contrasts markedly with that of turbines T4, T5, and T6 in the red-box group, which exhibit pronounced disparities under the same wind direction.

In the SW direction, which is nearly perpendicular to SE, the wake orientation aligns with the row formed by T2, T5, and T8. This alignment leads to greater divergence in both power output and DEL among the three turbines, reflecting the stronger sensitivity of their loading characteristics to wake sequencing when the wake is directed along their streamwise alignment. However, because the SW direction occurs with relatively low frequency, its contribution to the weighted metrics is much less apparent after accounting for directional probability.

These observations indicate that, from a long-term perspective, the influence of turbine wakes on annual power production and structural loading must be evaluated in conjunction with the wind-direction distribution of the specific site. Only by considering both wake severity and directional occurrence can the cumulative impact on wind farm performance be accurately assessed.

3.3. Structural integrity results

3.3.1. Fatigue crack growth

Fig. 16 presents a comparison of fatigue crack growth across nine turbines subjected to wake effects and a single turbine simulation where

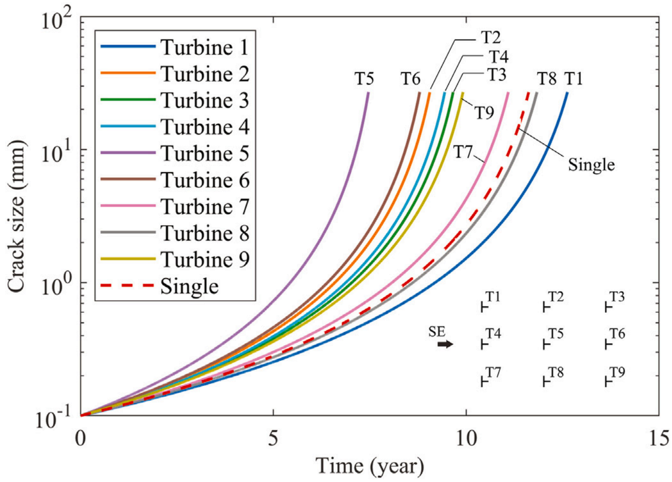

Fig. 16. Fatigue crack growth comparison among nine wind turbine structures and simulation without wake effects.

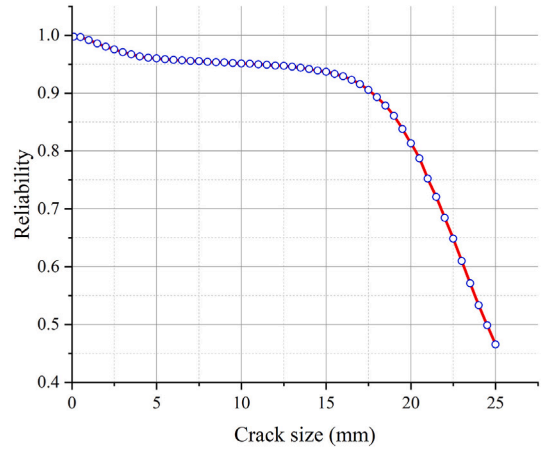

Fig. 17. Reliability degradation of the tower with increasing crack size.

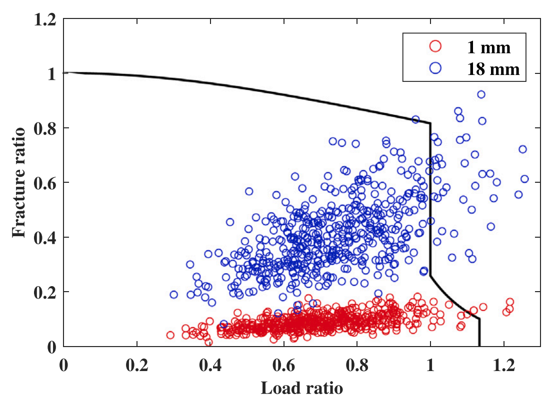

Fig. 18. Example Monte Carlo simulation results of the engineering critical assessment with different crack sizes (black line: FAL).

wake effects are not considered. While all curves exhibit the expected nonlinear growth characteristic of fatigue crack propagation in accordance with the Paris' law, there is significant variation in the crack growth rates among the individual turbines. Notably, Turbine 1 shows the slowest crack growth, with a 25 mm depth crack forming after approximately 12.6 years of operation, whereas Turbine 5 exhibits the fastest crack propagation, reaching through-thickness crack after just 7.4 years. The single-turbine simulation, which excludes the wake effects, results in a crack growth rate that lies between the slowest and fastest wake-influenced cases (closer to the slowest case), with through-thickness failure occurring at 11.6 years. In other words, the structure lifetimes vary from -36.2% to $+8.6\%$ under wake effects compared to the single-turbine simulation. If such a simulation is used to inform inspection and maintenance planning, it may lead to a significantly delayed intervention, increasing the risk of undetected damage progression and potentially catastrophic failure. Likewise, an overly conservative inspection and maintenance plan may be applied to turbines operating under significantly less severe loading conditions, leading to inefficient use of resources. Overall, this comparison highlights that wake effects can cause substantial differences in structural degradation, which may have significant implications for maintenance planning and optimization. Analysis of the associated loading characteristics suggests that this is influenced not only by differences in loading magnitude but also by variations in loading rate, with some turbines experiencing a higher number of dynamic load cycles within the same service life, which is more detrimental to the fatigue performance.

3.3.2. Crack acceptability and structural reliability

Fig. 17 illustrates the relationship between crack size and structural reliability. A clear decreasing trend is observed, characterized by three stages of degradation. When the crack size is less than approximately 5 mm, the reduction in reliability is modest. Beyond this point, the rate of decrease slows down, indicating that further crack growth does not lead to a substantial reduction in reliability. Up to a crack size of about 15–16 mm, the structural reliability remains above 0.9. However, once the crack size exceeds this threshold, further growth results in a pronounced decline in structural reliability. This nonlinear degradation behavior can be attributed to the inherent nonlinearity of the FAD, which establishes the failure assessment line and evaluates the assessment point by jointly considering fracture mechanics and plastic collapse criteria. As illustrated in Fig. 18, the structural response transitions from plastic collapse-dominated failure at small crack sizes to combined plastic collapse and fracture failure at larger crack sizes.

This observation underscores the importance of recognising damage tolerance in structural integrity management. The relatively slow rate of reliability degradation at intermediate crack sizes indicates that the structure retains a considerable margin of tolerance to damage in this regime, such that inspection or intervention may not be immediately necessary from a structural integrity perspective. In contrast, once the failure is considerably influenced by fracture, reliability may deteriorate rapidly, highlighting the critical importance of timely inspection and intervention before crack sizes approach this threshold. If decision-making is guided solely by crack size, without accounting for its structural acceptability and tolerance, these insights will be overlooked and the resulting decisions may be sub-optimal.

3.4. Operation and maintenance results

Based on the previous wake effect simulations and the derived crack propagation results of individual turbines, this section presents the O&M optimization results of the offshore wind farm, along with a comparative analysis.

3.4.1. Optimization results

By applying the multi-objective optimization algorithm NSGA-II, a set of solutions balancing cost minimization and reliability maximization is obtained. Fig. 19 illustrates the optimization process. As the number of iterations increases, the population gradually converges toward a stable state, suggesting that the obtained results are reliable. The multi-objective optimization yields a set of trade-off solutions that are mutually non-dominated, collectively forming the Pareto front, as they

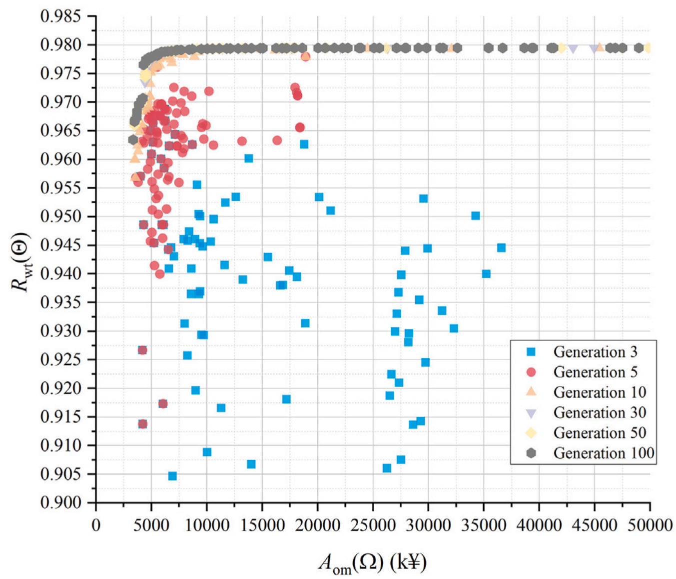

Fig. 19. Convergence process of populations as the number of generations increases.

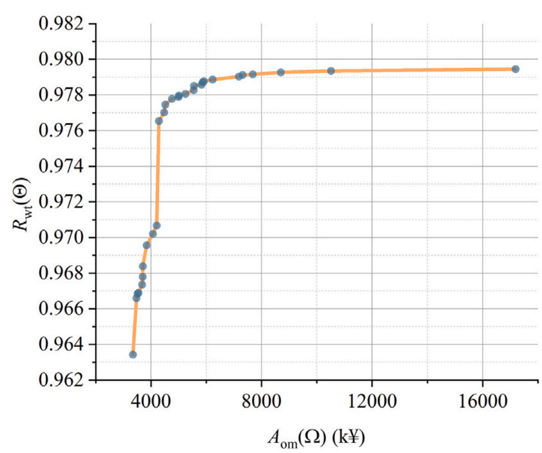

Fig. 20. Pareto front at the 100th generation.

outperform all other solutions across one objective. The Pareto front formed by all non-dominated solutions at the 100th generation is illustrated in Fig. 20. It consists of two priority solutions, namely a cost priority solution and a reliability priority solution, and compromise solutions between them. The values of the decision variables at the Pareto front are listed in Table 9. It is observed that the cost priority solution yields a value of A_{om} = 3346.8 k¥and R_{wt} = 0.9634 and the reliability priority solution shows a value of A_{om} = 17,192.8 k¥and R_{wt} = 0.9795. The performance of the remaining solutions lies between those of the two priority ones.

These solutions provide practical guidance for offshore wind farm O&M decision-making. If cost minimization is the primary concern, a cost-priority strategy can be adopted, accepting lower but still acceptable reliability in exchange for reduced maintenance expenditure. If reliability is prioritized, reliability-priority solutions become preferable, as they maximize turbine reliability and reduce the risk of unexpected failures under less restrictive budget constraints. When both cost and reliability matter, compromise solutions offer a balanced strategy that manages the trade-off between the two objectives without excessively sacrificing either. It should be noted that this Pareto front is derived under a deterministic setting, namely under the assumptions that the turbine states are fully observable and the model parameters are accurately known. If uncertainty is further introduced, such as parameter imprecision or partial state observability, the Pareto front is expected to, according to a previous study [107], become more dispersed and span a wider range.

3.4.2. Comparative analysis

The optimization results presented in Section 3.4.1 are based on a scenario that accounts for the wake-induced differences in crack growth among turbines at different locations. To highlight the impact of the variations in degradation rates on maintenance performance, we perform a comparative analysis between the approaches considering and ignoring degradation variations.

Existing studies on maintenance planning for load-induced cracks have been conducted mainly at the single-turbine level, where only the degradation process of an individual turbine is considered, while the farm-level interactions and state heterogeneity among turbines are largely neglected. When the optimized maintenance strategy derived under such a single-turbine scenario is directly extended to the wind-farm level, a potential mismatch arises. This is because the maintenance strategy can be essentially regarded as a state-triggered decision mechanism defined by the decision variables ($\varphi_p, \varphi_o, \zeta$). Such a decision mechanism is derived based on a single, homogeneous degradation pattern. In a real offshore wind farm, however, wake effects induce different structural degradation rates and trajectories across turbines. Therefore, this maintenance strategy may become inappropriate at the farm scale, potentially resulting in under-maintenance for more severely degraded turbines and over-maintenance for less affected ones.

To quantify the decision bias induced by neglecting degradation heterogeneity, a multi-objective optimization scenario is constructed,

Table 9
Optimized values of the decision variables in the Pareto front.

No	φ_p(mm)	φ_o(mm)	ζ(day)	A_{om} (k¥)	R_{wt}	No	φ_p(mm)	φ_o(mm)	ζ(day)	A_{om} (k¥)	R_{wt}
1	2.27	0.30	813	3346.8	0.9634	16	0.66	0.18	366	5007.9	0.9780
2	3.83	0.30	610	3473.7	0.9666	17	0.67	0.21	306	5245.5	0.9781
3	2.50	0.34	609	3510.2	0.9668	18	0.47	0.15	782	5546.4	0.9783
4	2.29	0.22	609	3546.6	0.9669	19	0.34	0.19	742	5556.6	0.9785
5	4.49	0.33	494	3678.7	0.9674	20	0.41	0.21	519	5829.3	0.9786
6	3.06	0.37	491	3699.3	0.9678	21	0.32	0.18	501	5870.5	0.9787
7	3.31	0.20	488	3703.8	0.9684	22	0.41	0.10	490	5913.0	0.9788
8	3.72	0.31	406	3842.3	0.9696	23	0.38	0.10	367	6226.2	0.9789
9	3.07	0.26	348	4067.0	0.9702	24	0.27	0.17	430	7180.5	0.9790
10	3.76	0.32	304	4208.5	0.9707	25	0.29	0.11	406	7314.2	0.9791
11	0.73	0.10	924	4288.2	0.9765	26	0.28	0.10	307	7684.7	0.9792
12	0.77	0.25	629	4477.3	0.9770	27	0.25	0.12	353	8696.2	0.9793
13	0.65	0.17	610	4516.2	0.9775	28	0.21	0.13	236	10,515.6	0.9794
14	0.67	0.18	457	4758.7	0.9778	29	0.15	0.10	124	17,192.8	0.9795
15	0.57	0.23	369	4994.7	0.9779						

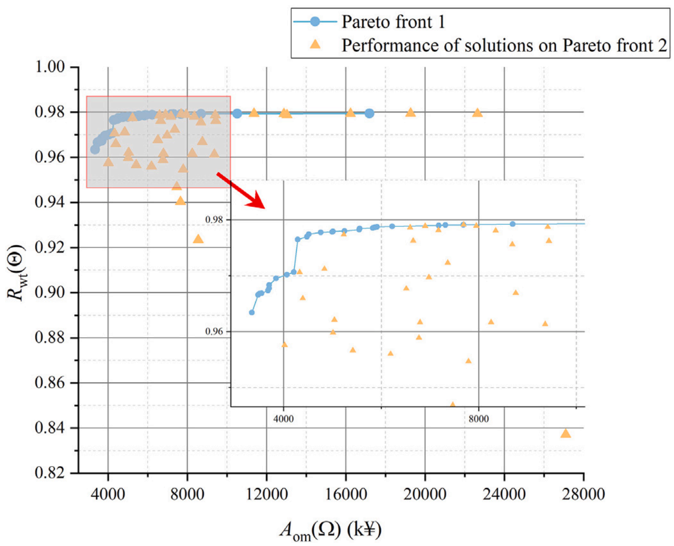

Fig. 21. Comparison of solutions considering and ignoring wake-induced crack growth variations.

in which the degradation differences among turbines are ignored, and the resulting Pareto set is referred to as Pareto front 2. It should be noted that the cost and reliability performance of the solutions on Pareto front 2 only represent their apparent optimality under the homogenized assumption, rather than their actual performance in a real wind farm. This is because the corresponding scenario assumes identical degradation evolution for all turbines and neglects the crack-growth differences induced by wake effects, which are unrealistic in practical operation.

The solutions on Pareto front 2 are re-evaluated under the scenario that accounts for wake-induced differences in crack propagation (i.e., the same scenario as in Fig. 20). The performance of these solutions is compared with that of the original Pareto front, referred to as Pareto front 1, in Fig. 21. This comparison reveals that Pareto front 1 completely dominates the solutions on Pareto front 2. In other words, maintenance strategies derived under the traditional approach, where wake-induced crack growth is ignored, lead to higher maintenance costs and lower reliability when applied to real-world scenarios that do include wake effects. Moreover, the solutions on Pareto front 2 exhibit a wide distribution. In some extreme cases, the reliability drops below 0.9, and the maintenance cost exceeds 24,000 k¥, indicating substantial risks. This highlights that neglecting wake effects and the resulting spatial variations in crack growth can lead to serious decision-making errors and significantly impair the overall maintenance performance of the offshore wind farm.

Further examining the entire solution sets, the average maintenance cost and reliability of the solutions on Pareto front 2 are 10,428.0 k¥and 0.9574, respectively, whereas those on Pareto front 1 are 5651.4 k¥and 0.9747. This indicates an average increase of 84.5% in cost and an average decrease of 1.8% in reliability. This comparison is demonstrated in Table 10. The underlying reason may lie in the failure to account for wake-induced crack growth variations, which leads to both under-maintenance and over-maintenance. Since most maintenance thresholds fall within a region where structural reliability is relatively insensitive to minor crack growth differences, the impact on reliability is limited. However, these thresholds have a direct and significant effect on maintenance triggering and associated costs. An inappropriate threshold setting can either result in overly frequent maintenance actions or in delayed maintenance leading to a high risk of structural failure, so substantial financial losses will be caused in these cases.

4. Conclusions and future work

Wake-induced heterogeneity in offshore wind farms is not merely a local aerodynamic issue, but a cross-layer problem whose consequences can accumulate from turbine-level operating differences to broader impacts on energy production, fatigue loading, structural deterioration, reliability, and lifecycle asset performance at the wind farm level. However, this propagation mechanism has not been systematically understood in the existing literature. To address this gap, this study has developed a comprehensive framework to systematically assess the multidimensional implications of wake-induced heterogeneity in offshore wind farms. The proposed framework couples three key models: (i) wake aerodynamics, modeled through joint wind condition distributions and a dynamic wake meandering model; (ii) structural integrity analysis, conducted via a physics-based crack growth model using Paris' law and probabilistic ECA; and (iii) maintenance management, enabled by a condition-based opportunistic maintenance model with multi-objective optimization of inspection and repair decisions.

A case study on the Akita offshore wind farm in Japan was used to demonstrate the applicability of the proposed framework. For the investigated representative 3×3 layout and the adopted modeling assumptions, the results indicate that wake-induced heterogeneity can have substantial multidimensional impacts on offshore wind farm performance, reducing overall energy production efficiency by 20.9%, increasing fatigue loading by 47.7%, inducing structural lifetime variations from -36.2% to $+8.6\%$ across turbines, lowering wind turbine reliability by 1.8%, and increasing lifecycle O&M costs by 84.5%. These findings suggest that incorporating wake-induced heterogeneity may provide a more informative basis for project appraisal, maintenance planning, and long-term asset management. However, the present case study should be interpreted as a proof-of-concept demonstration rather than a full-scale validation. Although the modular framework is conceptually extendable to larger wind farms, further work is required to examine its scalability, computational efficiency, and robustness under different layouts, environmental conditions, turbine types, and maintenance settings.

Several directions deserve further investigation in future. First, although this study focuses on tower crack growth, the framework can be extended to other key components, such as blades and mooring systems, which involve different degradation mechanisms and maintenance requirements. Second, the current framework assumes fully known wake-induced loading histories, whereas in practice such information may be uncertain or only partially observable. This could be addressed in future work by incorporating state-estimation methods, such as Bayesian inference, Kalman filtering, or particle filtering, to support real-time degradation tracking under uncertainty. Third, a finer discretization of wind speed and wind direction may further improve the accuracy of site-specific lifetime fatigue estimation and will be investigated in future work. Finally, beyond cost and reliability, future studies may incorporate environmental metrics, such as vessel

Table 10
Performance comparison of solutions considering and ignoring wake-induced crack growth variations.

	Pareto front 1			Solutions on Pareto front 2		
	Cost priority	Reliability priority	Average	Cost priority	Reliability priority	Average
Maintenance costs (k¥)	3346.8	17,192.8	5651.4	27,100.0	19,266.2	10,428.0
Reliability	0.9634	0.9795	0.9747	0.8371	0.9795	0.9574

emissions or the lifecycle carbon footprint of maintenance, to support more sustainability-oriented assessments.

CRediT authorship contribution statement

Mingxin Li: Writing – original draft, Methodology, Investigation, Formal analysis, Conceptualization. **Yun-Peng Song:** Writing – original draft, Software, Methodology, Investigation, Formal analysis, Conceptualization. **Guiyu Cao:** Writing – review & editing, Methodology, Conceptualization. **Yuka Kikuchi:** Writing – review & editing, Investigation, Formal analysis. **Jonas W. Ringsberg:** Writing – review & editing, Methodology, Formal analysis. **Matthias G.R. Faes:** Writing – review & editing, Methodology, Formal analysis. **Jeom Kee Paik:** Writing – review & editing. **You Dong:** Writing – review & editing. **Jichuan Kang:** Writing – review & editing. **Shen Li:** Writing – original draft, Software, Methodology, Investigation, Formal analysis, Conceptualization.

Declaration of competing interest

The authors declare that they have no known competing financial interests or personal relationships that could have appeared to influence the work reported in this paper.

Acknowledgements

The author, Dr. Mingxin Li, is an International Research Fellow of Japan Society for the Promotion of Science (Postdoctoral Fellowships for Research in Japan (Standard)). This research is financially supported by the JSPS KAKENHI Grant Number 24KF0134.

Data availability

The authors do not have permission to share data.

References

[1] Wang F, Harindintwali JD, Yuan Z, Wang M, Wang F, Li S, Yin Z, Huang L, Fu Y, Li L, et al. Technologies and perspectives for achieving carbon neutrality. Innovation 2021;2(4).

[2] Yin M, Ji R, Zhu R, Sun K, Zhang J, Cheng Y, Zhang Y, Reabroy R. High-fidelity IDDES simulations of unsteady hydrodynamics and wake evolution characteristics of a tidal current turbine under focused wave-current interaction. Renew Energy 2026;125647.

[3] Oladapo BI, Olawumi MA, Olugbade TO, Ismail SO. Data analytics driving net zero tracker for renewable energy. Renew Sustain Energy Rev 2025;208(115061).

[4] Li C., Mogollón JM, Tukker A, Dong J, von Terzi D, Zhang C, Steubing B. Future material requirements for global sustainable offshore wind energy development. Renew Sustain Energy Rev 2022;164(112603).

[5] Moussavi S, Barutha P, Dvorak B. Environmental life cycle assessment of a novel offshore wind energy design project: a United States based case study. Renew Sustain Energy Rev 2023;185(113643).

[6] Li D, Zhao J, Wu Y, Zhang Y, Liang H. An innovative bionic offshore wind foundation: scaled suction caisson. Renew Sustain Energy Rev 2024;191(114208).

[7] Williams R, Zhao F, Melkonyan N, Hutchinson M, Cheong J. Global offshore wind report 2025. Technical report. Lisbon, Portugal: Global Wind Energy Council; 2025.

[8] Xu X, Shen X, Wang S, Xing Y, Yang P, Ye Y, Ji R, Xu L. Effects of wake-added turbulence on extreme loads and fatigue damage of floating offshore wind turbines. Phys Fluids 2025;37(10).

[9] Zhang T, Xu X, Wang S, Xing Y, Dou P, Ji R, Yang P. Investigation of wake steering control effects on the dynamic responses of 15 MW semi-submersible floating wind farms. Renew Energy 2025;254(123704).

[10] Pryor SC, Barthelmie RJ, Shepherd TJ. Wind power production from very large offshore wind farms. Joule 2021;5(10):2663–86.

[11] Baas P, Verzijlbergh R, van Dorp P, Jonker H. Investigating energy production and wake losses of multi-gigawatt offshore wind farms with atmospheric large-eddy simulation. Wind Energy Sci 2023;8(5):787–805.

[12] Li B, He J, Ge M, Ma H, Du B, Yang H, Liu Y. Study of three wake control strategies for power maximization of offshore wind farms with different layouts. Energy Convers Manag 2022;268(116059).

[13] Li M, Kikuchi Y. Predictive maintenance optimization for offshore wind farms with power losses and wake effect considerations. In: ISOPE international ocean and polar engineering conference, ISOPE–I. ISOPE; 2025.

[14] Zhang J, Zuo H, Zhu S, Yang J, Lu L. Fatigue degradation of wind turbines considering dynamic wake meandering effects. Eng Struct 2024;300(117132).

[15] Zhang J, Heng J, Dong Y, Baniotopoulos C, Yang Q. Coupling multi-physics models to corrosion fatigue prognosis of high-strength bolts in floating offshore wind turbine towers. Eng Struct 2024;301(117309).

[16] Vieira M, Henriques E, Snyder B, Reis L. Insights on the impact of structural health monitoring systems on the operation and maintenance of offshore wind support structures. Struct Saf 2022;94(102154).

[17] Li H, Soares CG. Assessment of failure rates and reliability of floating offshore wind turbines. Reliab Eng Syst Saf 2022;228(108777).

[18] Dao C, Kazemtabrizi B, Crabtree C. Wind turbine reliability data review and impacts on levelised cost of energy. Wind Energy 2019;22(12):1848–71.

[19] Hou G, Xu K, Lian J. A review on recent risk assessment methodologies of offshore wind turbine foundations. Ocean Eng 2022;264(112469).

[20] Sebastiani A, Castellani F, Crasto G, Segalini A. Data analysis and simulation of the lillgrund wind farm. Wind Energy 2021;24(6):634–48.

[21] Ltd. Japan Wind Development Co. Emergency inspections in response to the tower collapse accident at rokkasho wind farm (units 1–3); 2023 https://www.jwd.co.jp/news/%E5%85%AD%E3%82%B1%E6%89%80%E6%9D%91%E9%A2%A8%E5%8A%9B%E7%99%BA%E9%9B%BB%E6%89%80-1-3%E5%8F%B7%E6%A9%9F%E3%82%BF%E3%83%AF%E3%83%BC%E5%80%92%E5%A3%8A%E4%BA%8B%E6%95%85%E7%99%BA%E7%94%9F%E3%82%92/ [Accessed 27 October 2025]. Published: 2023-04-07; partial update on 2023-04-26. Page in Japanese.

[22] Larsen GC, Madsen HA, Thomsen K, Larsen TJ. Wake meandering: a pragmatic approach. Wind Energy 2007;10(6):575–87.

[23] Madsen HA, Larsen GC, Ott S, Sørensen JN. Modelling of wake meandering and its influence on wind turbine loading. Wind Energy 2010;13(4):573–85.

[24] Keck R-E, Veldkamp H. A dynamic wake meandering model for power and load predictions. Wind Energy 2012;15(7):1041–52.

[25] Fleming PA, Gebraad PMO, Lee S, van Wingerden J-W, Johnson K, Churchfield M, Michalakes J, Spalart P, Moriarty P. Evaluating techniques for redirecting turbine wakes using SOWFA. Renew Energy Oct 2014;70:211–8.

[26] Martínez-Tossas LA, Meneveau C. Filtered actuator disk modeling of wind turbine wake dynamics in large wind farms. Phys Fluids 2019;31(8):085108.

[27] Qian G-W, Song Y-P, Ishihara T. A control-oriented large eddy simulation of wind turbine wake considering effects of coriolis force and time-varying wind conditions. Energy Jan 2022;239(121876).

[28] Dammann T, Dangi N, Van Wingerden J-W, Yu W. Benchmark study on rotor performance, wake dynamics, and atmospheric boundary layers using NREL SOWFA-6 and AMR-WIND. J Phys Conf Ser May 2025;3016(1):012034. IOP Publishing.

[29] Liu Z, Li Q, Ishihara T, Peng J. Numerical simulations of fatigue loads on wind turbines operating in wakes. Wind Energy 2020;23(5):1301–16.

[30] Rinker JM, Sagredo ES, Bergami L. The importance of wake meandering on wind turbine fatigue loads in wake. Energies 2021;14(21).

[31] Song Y-P, Ishihara T. A novel dynamic wake model for prediction of wind speed and power production considering wake propagation velocity and deflection. Appl Energy 2025;400(126526).

[32] Wang C, Muñóz-Simon A, Deskos G, Laizet S, Palacios R, Campagnolo F, Bottasso CL. Code-to-code-to-experiment validation of LES-ALM wind farm simulators. J Phys Conf Ser Sep 2020;1618(6):062041. IOP Publishing.

[33] Becker M, Allaerts D, van Wingerden JW. Ensemble-based flow field estimation using the dynamic wind farm model FLORIDyn. In: Energies, vol. 15(22). MDPI, Nov 2022.

[34] Shaler K, Jonkman J. FAST.Farm development and validation of structural load prediction against large eddy simulations. In: Wind energy, vol. 24(5). John Wiley and Sons Ltd, May 2021. p. 428–49.

[35] Reinwardt I, Schilling L, Dalhoff P, Steudel D, Breuer M. Dynamic wake meandering model calibration using nacelle-mounted LiDAR systems. In: Wind energy science, vol. 5(2). Copernicus GmbH, Jun 2020. p. 775–92.

[36] International Electrotechnical Commission. IEC 61400-1:2019 wind energy generation systems – Part 1: design requirements. 2019. https://webstore.iec.ch/publication/60225. 3.0, Geneva, Switzerland.

[37] Bastankhah M, Porté-Agel F. Experimental and theoretical study of wind turbine wakes in yawed conditions. J Fluid Mech 2016;806:506–41.

[38] Reinwardt I, Gerke N, Dalhoff P, Steudel D, Moser W. Validation of wind turbine wake models with focus on the dynamic wake meandering model. J Phys Conf Ser 2018;1037(7).

[39] Yang X, Sotiropoulos F. A review on the meandering of wind turbine wakes. Energies 2019;12(24).

[40] Larsen TJ, Larsen GC, Pedersen MM, Enevoldsen K, Madsen HA. Validation of the dynamic wake meander model with focus on tower loads. J Phys Conf Ser 2017;854(1):012027. https://doi.org/10.1088/1742-6596/854/1/012027.

[41] Song Y-P, Ishihara T. A study of wake effects on fatigue loads of turbines considering spatiotemporal wind data and rotational speed control effect. J Wind Eng Ind Aerodyn 2026;274(106458).

[42] Lanzilao L, Meyers J. A wake-merging method for wind-farm power prediction in the presence of heterogeneous background velocity fields. Wind Energy 2020;23(8):1681–702.

[43] Qian GW, Ishihara T. Wind farm power maximization through wake steering with a new multiple wake model for prediction of turbulence intensity. In: Energy, vol. 220. Elsevier Ltd; 2021:119680.

[44] Zwick D, Muskulus M. Simplified fatigue load assessment in offshore wind turbine structural analysis. Wind Energy 2016;19(2):265–78.

[45] Gaidai O, Yakimov V, Wang F, Zhang F, Balakrishna R. Floating wind turbines structural details fatigue life assessment. Sci Rep 2023;13(16312).

[46] Mehmanparast A, Chahardehi A, Brennan F, Manzocchi M. Re-evaluation of fatigue design curves for offshore wind monopile foundations using thick as-welded test specimens. Eng Fail Anal 2024;158(107971).

[47] Velarde J, Kramhøft C, Sørensen JD. Global sensitivity analysis of offshore wind turbine foundation fatigue loads. Renew Energy 2019;140:177–89.

[48] Dong W, Moan T, Gao Z. Long-term fatigue analysis of multi-planar tubular joints for jacket-type offshore wind turbine in time domain. Eng Struct 2011;33(6):2002–14.
[49] Li X, Zhang W. Long-term fatigue damage assessment for a floating offshore wind turbine under realistic environmental conditions. Renew Energy 2020;159:570–84.
[50] Kvittem MI, Moan T. Time domain analysis procedures for fatigue assessment of a semi-submersible wind turbine. Mar Struct 2015;40:38–59.
[51] Barrera C, Battistella T, Guanche R, Losada IJ. Mooring system fatigue analysis of a floating offshore wind turbine. Ocean Eng 2020;195(106670).
[52] Horn J-T, Leira BJ. Fatigue reliability assessment of offshore wind turbines with stochastic availability. Reliab Eng Syst Saf 2019;191(106550).
[53] Velarde J, Kramhøft C, Sørensen JD, Zorzi G. Fatigue reliability of large monopiles for offshore wind turbines. Int J Fatigue 2020;134(105487).
[54] Wilkie D, Galasso C. Gaussian process regression for fatigue reliability analysis of offshore wind turbines. Struct Saf 2021;88(102020).
[55] DNV. DNV-RP-C203: fatigue design of offshore steel structures. Recommended practice, edition 2024-10. DNV; 2024.
[56] Straub D, Faber MH. Computational aspects of risk-based inspection planning. Comput-Aided Civ Infrastruct Eng 2006;21(3):179–92.
[57] Amirafshari P, Brennan F, Kolios A. A fracture mechanics framework for optimising design and inspection of offshore wind turbine support structures against fatigue failure. Wind Energy Sci 2021;6(3):677–99.
[58] Mehmanparast A, Brennan F, Tavares I. Fatigue crack growth rates for offshore wind monopile weldments in air and seawater: SLIC inter-laboratory test results. Mater Des 2017;114:494–504.
[59] Li S, Brennan F. Implementation of digital twin-enabled virtually monitored data in inspection planning. Appl Ocean Res 2024;144(103903).
[60] Dong W, Moan T, Gao Z. Fatigue reliability analysis of the jacket support structure for offshore wind turbine considering the effect of corrosion and inspection. Reliab Eng Syst Saf 2012;106:11–27.
[61] Zhu F, Yeter B, Brennan F, Collu M. Time-domain fatigue reliability analysis for floating offshore wind turbine substructures using coupled nonlinear aero-hydro-servo-elastic simulations. Eng Struct 2024;318(118759).
[62] British Standards Institution. BS 7910:2019: Guide to methods for assessing the acceptability of flaws in metallic structures. British Standard. BSI; 2019. https://doi.org/10.3403/30369478.
[63] He M, Pang M, Chen NZ. Engineering critical assessment (ECA) for monopile foundation of an offshore wind turbine subjected to pitting. Ocean Eng 2023;285(115400).
[64] Zhang T, Xiaosen X, Wang S, Xing Y, Dou P, Ji R, Yang P. Investigation of wake steering control effects on the dynamic responses of 15MW semi-submersible floating wind farms. Renew Energy 2025;254(123704).
[65] Hameed Z, Ahn S-H, Cho YM. Practical aspects of a condition monitoring system for a wind turbine with emphasis on its design, system architecture, testing and installation. Renew Energy 2010;35(5):879–94.
[66] de Jonge B, Teunter R, Tinga T. The influence of practical factors on the benefits of condition-based maintenance over time-based maintenance. Reliab Eng Syst Saf 2017;158:21–30.
[67] Nielsen JJ, Sørensen JD. On risk-based operation and maintenance of offshore wind turbine components. Reliab Eng Syst Saf 2011;96(1):218–29.
[68] Sindi A, Kim HJ, Yang YJ, Thomas G, Paik JK. Advancing digital healthcare engineering for aging ships and offshore structures: an in-depth review and feasibility analysis. Data-Centric Eng 2024;5:e18.
[69] Li M, Jiang X, Carroll J, Negenborn RR. Operation and maintenance management for offshore wind farms integrating inventory control and health information. Renew Energy 2024;231(120970).
[70] Oh SY, Joung C, Lee S, Shim Y-B, Lee D, Cho G-E, Jang J, Lee IY, Park YB. Condition-based maintenance of wind turbine structures: a state-of-the-art review. Renew Sustain Energy Rev 2024;204(114799).
[71] Koukoura S, Scheu MN, Kolios A. Influence of extended potential-to-functional failure intervals through condition monitoring systems on offshore wind turbine availability. Reliab Eng Syst Saf 2021;208(107404).
[72] Wang M, Wang C, Hnydiuk-Stefan A, Feng S, Atilla I, Li Z. Recent progress on reliability analysis of offshore wind turbine support structures considering digital twin solutions. Ocean Eng 2021;232(109168).
[73] Hussain M, Mirjat NH, Shaikh F, Dhirani LL, Kumar L, Sleiti AK. Condition monitoring and fault diagnosis of wind turbine: a systematic literature review. IEEE Access 2024;12:190220–39. https://doi.org/10.1109/ACCESS.2024.3514747.
[74] Li M, Kikuchi Y, Ringsberg JW, Gryllias KC, Baraldi P, Zio E, Carroll J. Empowering digital twins for wind energy operation and maintenance: a prospective framework and future directions. Renew Sustain Energy Rev 2026;235(116970).
[75] Yang Y, Liang F, Zhu Q, Zhang H. An overview on structural health monitoring and fault diagnosis of offshore wind turbine support structures. J Mar Sci Eng 2024;12(3):377.
[76] Xie Y, Kim HJ, Yin Y, Liu K, Smith T, Paik JK. Enhancing the safety and sustainability of aging jacket-type offshore wind turbines in extreme weather conditions through digital healthcare engineering: a literature review. Sh Offshore Struct 2025;1–28.
[77] Zhang J, Guo H, Jafari-Asl J, Dong Y, Bastidas-Arteaga E, Cui H. Multi-physical driven time-dependent reliability analysis framework for reinforced concrete floating wind turbine foundations considering climate change. Thin-Walled Struct 2025;213(113309).
[78] Li M, Xu Z, Li S, Kikuchi Y, Dong Y, Gryllias KC, Baraldi P, Zio E, Carroll J. Health prognostics and maintenance decision-making for wind energy: a comprehensive overview. Renew Sustain Energy Rev 2026;226(116269).
[79] Xia J, Zou G. Operation and maintenance optimization of offshore wind farms based on digital twin: a review. Ocean Eng 2023;268(113322).
[80] Sindi A, Paik J-K. Digital healthcare engineering system for enhancing the safety and sustainability of aging monopile offshore wind turbines in storm conditions. In: SNAME maritime convention. SNAME; 2025, D021S009R001.
[81] Mehrjoo A, Song M, Moaveni B, Papadimitriou C, Hines E. Optimal sensor placement for parameter estimation and virtual sensing of strains on an offshore wind turbine considering sensor installation cost. Mech Syst Signal Process 2022;169(108787).
[82] Li M, Kefal A, Oterkus E, Oterkus S. Structural health monitoring of an offshore wind turbine tower using ifem methodology. Ocean Eng 2020;204(107291).
[83] Xu Y, Nikitas G, Zhang T, Han Q, Chryssanthopoulos M, Bhattacharya S, Wang Y. Support condition monitoring of offshore wind turbines using model updating techniques. Struct Health Monit 2020;19(4):1017–31.
[84] Xu JT, Luo L, Saw J, Wang C-C, Sinha SK, Wolfe R, Soga K, Wu Y, DeJong M. Structural health monitoring of offshore wind turbines using distributed acoustic sensing (DAS). J Civ Struct Health Monit 2025;15(2):445–63.
[85] Xiang Z-Q, Wang J-T, Wang W, Pan J-W, Liu J-F, Le Z-J, Cai X-Y. Vibration-based health monitoring of the offshore wind turbine tower using machine learning with Bayesian optimisation. Ocean Eng 2024;292(116513).
[86] Wang Z, Qiao D, Tang G, Wang B, Yan J, Ou J. An identification method of floating wind turbine tower responses using deep learning technology in the monitoring system. Ocean Eng 2022;261(112105).
[87] Feng W-Q, Mousavi Z, Farhadi M, Bayat M, Ettefagh MM, Varahram S, Sadeghi MH. A hybrid wavelet-deep learning approach for vibration-based damage detection in monopile offshore structures considering soil interaction. J Civ Struct Health Monit 2025;15(2):417–44.
[88] Farhan M, Schneider R, Thöns S. Predictive information and maintenance optimization based on decision theory: a case study considering a welded joint in an offshore wind turbine support structure. Struct Health Monit 2022;21(1):185–207.
[89] Yan R, Dunnett S, Jackson L. Impact of condition monitoring on the maintenance and economic viability of offshore wind turbines. Reliab Eng Syst Saf 2023;238(109475).
[90] Kong S, Liu Y. Model predictive control for risk-based inspection and maintenance planning of offshore wind turbines. Sh Offshore Struct 2025;1–12.
[91] Hlaing N, Morato PG, Nielsen JS, Amirafshari P, Kolios A, Rigo P. Inspection and maintenance planning for offshore wind structural components: integrating fatigue failure criteria with Bayesian networks and Markov decision processes. Struct Infrastruct Eng 2022;18(7):983–1001.
[92] De Jonge B, Scarf PA. A review on maintenance optimization. Eur J Oper Res 2020;285(3):805–24.
[93] Li M, Wang M, Kang J, Sun L, Jin P. An opportunistic maintenance strategy for offshore wind turbine system considering optimal maintenance intervals of subsystems. Ocean Eng 2020;216(108067).
[94] Kang J, Soares CG. An opportunistic maintenance policy for offshore wind farms. Ocean Eng 2020;216(108075).
[95] Lu Y, Sun L, Zhang X, Feng F, Kang J, Fu G. Condition based maintenance optimization for offshore wind turbine considering opportunities based on neural network approach. Appl Ocean Res 2018;74:69–79.
[96] Zhao H, Xu F, Liang B, Zhang J, Song P. A condition-based opportunistic maintenance strategy for multi-component system. Struct Health Monit 2019;18(1):270–83.
[97] Gan J, Zhang W, Wang S, Zhang X. Joint decision of condition-based opportunistic maintenance and scheduling for multi-component production systems. Int J Prod Res 2022;60(17):5155–75.
[98] Zhou P, Yin PT. An opportunistic condition-based maintenance strategy for offshore wind farm based on predictive analytics. Renew Sustain Energy Rev 2019;109:1–9.
[99] Zhang X, Tao J, Noshadravan A. Probabilistic digital twin for reliability-based maintenance optimization of offshore wind turbines. Renew Energy 2026;256(123777).
[100] Gintautas T, Sørensen JD. Reliability-based inspection planning of 20 MW offshore wind turbine jacket. Int J Offshore Polar Eng 2018;28(3):272–9.
[101] Yeter B, Garbatov Y, Soares CG. Risk-based maintenance planning of offshore wind turbine farms. Reliab Eng Syst Saf 2020;202(107062).
[102] Rangel-Ramírez JG, Sørensen JD. Risk-based inspection planning optimisation of offshore wind turbines. Struct Infrastruct Eng 2012;8(5):473–81.
[103] Zhong S, Pantelous AA, Goh M, Zhou J. A reliability-and-cost-based fuzzy approach to optimize preventive maintenance scheduling for offshore wind farms. Mech Syst Signal Process 2019;124:643–63.
[104] Paris P, Erdogan F. A critical analysis of crack propagation laws. J Basic Eng 1963;85(4):528–33.
[105] Newman JC, Raju IS. An empirical stress-intensity factor equation for the surface crack. Eng Fract Mech 1981;15(1):185–92.
[106] Tanwar M, Rai RN, Bolia N. Imperfect repair modeling using kijima type generalized renewal process. Reliab Eng Syst Saf 2014;124:24–31.
[107] Li M, Jiang X, Carroll J, Negenborn RR. A multi-objective maintenance strategy optimization framework for offshore wind farms considering uncertainty. Appl Energy 2022;321(119284).
[108] Deb K, Pratap A, Agarwal S, Meyarivan TAMT. A fast and elitist multiobjective genetic algorithm: NSGA-II. IEEE Trans Evol Comput 2002;6(2):182–97.
[109] Memija A. Japan's first commercial-scale offshore wind farm fully up and running. offshoreWIND.biz, 31 January; 2023. Available at: https://www.offshorewind.biz/2023/01/31/japans-first-commercial-scale-offshore-wind-farm-fully-up-and-running/ [accessed 20 July 2026].
[110] Jonkman BJ, Butterfield S, Musial W, Scott G. Definition of a 5-MW reference wind turbine for offshore system development. Technical Report NREL/TP-500-38060 National Renewable Energy Laboratory; 2009.

[111] New Energy and Industrial Technology Development Organization (NEDO). NeoWins (offshore wind map); 2018. Last updated: 2018-03-30; https://appwdc1.infoc.nedo.go.jp/Nedo_Webgis/top.html [Accessed 8 August 2025].

[112] Farhan M, Schneider R, Thöns S, Gündel M. Probabilistic cost modeling as a basis for optimizing inspection and maintenance of turbine support structures in offshore wind farms. Wind Energy Sci 2025;10(2):461–81.

[113] Stehly T, Duffy P. 2020 cost of wind energy review. Technical report Golden, CO (United States): National Renewable Energy Laboratory (NREL); 2021.

[114] Long L, Mai QA, Morato PG, Sørensen JD, Thöns S. Information value-based optimization of structural and environmental monitoring for offshore wind turbines support structures. Renew Energy 2020;159:1036–46.

[115] Li M, Bijvoet B, Wu K, Jiang X, Negenborn RR. Optimal chartering decisions for vessel fleet to support offshore wind farm maintenance operations. Ocean Eng 2024;298(117202).

[116] Li M, Jiang X, Negenborn RR. Opportunistic maintenance for offshore wind farms with multiple-component age-based preventive dispatch. Ocean Eng 2021;231(109062).

[117] Chen T, Wang X, Yuan G, Liu J. Fatigue bending test on grouted connections for monopile offshore wind turbines. Mar Struct 2018;60:52–71.

[118] Jonkman J. B. TurbSim user's guide: version 1.50. Technical Report NREL/TP-500-46198 Golden, CO, USA: National Renewable Energy Laboratory; Sep 2009 [Revised 26 August 2009].